AGU100 ADVANCING EARTH AND SPACE SCIENCE

Water Resources Research

RESEARCH ARTICLE
10.1029/2018WR022808

Key Points:
- Estimation of friction velocity (u^*) using surface renewal analysis (SRA) is presented
- SRA offers advantages to estimate the surface heat flux
- SRA is useful to estimate parameters required for land surface modeling

Correspondence to:
F. Castellví,
f-castellvi@macs.udl.cat

Citation:
Castellví, F. (2018). An advanced method based on surface renewal theory to estimate the friction velocity and the surface heat flux. *Water Resources Research*, *54*. https://doi.org/10.1029/2018WR022808

Received 19 FEB 2018
Accepted 12 NOV 2018
Accepted article online 19 NOV 2018

An Advanced Method Based on Surface Renewal Theory to Estimate the Friction Velocity and the Surface Heat Flux

F. Castellví[1]

[1]Department of Environment and Soil Sciences, University of Lleida, Lleida, Spain

Abstract The earlier formulation based on surface renewal (SR) analysis for estimating the sensible (or buoyant) heat flux (H) of a surface without requiring calibration involved canopy parameters to simultaneously estimate H and the friction velocity (u_*). A SR-based formulation is derived that allows estimating u_* and subsequently H that, at most, involves the zero-plane displacement. Regardless of the measurement height above the canopy and the stability case, u_* and H estimates were closed to values measured using the eddy covariance method for either homogeneous or sparse (orchards) canopies. The proposed SR analysis can be potentially considered for gap filling in half-hourly eddy covariance series of u_* and H and to estimate parameters useful for land surface modeling, such as the roughness length for momentum, the roughness lengths for momentum, and heat and the turbulent Prandtl number.

1. Introduction

During the last six decades indirect methods and approaches have been developed to simultaneously estimate the surface friction velocity and the sensible heat flux on the basis of Monin-Obukhov Similarity Theory (MOST). Often (i.e., for field applications), because the mean wind speed is a standard measurement in agricultural areas, the friction velocity has been estimated on the basis of the wind log-law, which involves the surface sensible heat flux and canopy parameters as input. The latter have been estimated using a variety of semiempirical relationships requiring different inputs, such as the canopy height, the leaf area index, and drag coefficients (Arnqvist & Bergström, 2014; Graefe, 2004; Jackson, 1981; Raupach, 1994).

The Surface Renewal (SR) theory is a simplification of surface turbulent flow exchange proposed by Higbie (1935) and subsequently modified by Danckwerts (1951), to study liquid-gas interfacial heat transfer in chemical engineering. The SR theory was the basis to derive new schemes and models to explain scalar exchange near-wall turbulent flows (Brutsaert, 1965; Bullin & Dukler, 1972; Harriot, 1962; Meek & Baer, 1970; Seo & Lee, 1988, among others), such as evaporation rates from different kind of surfaces (e.g., free water surfaces, rough surfaces, and porous media) (Brustasert, 1965, 1975; Haghighi & Or, 2013; Katul & Liu, 2017). In conjunction with the analysis of scalar concentration time series sampled at high frequency, based on the role of large coherent motions, a different SR-based depiction was introduced by Paw U et al. (1995) for estimating the eddy flux of a scalar over agricultural and forest surfaces without requiring measurements of the wind speed and estimation of canopy parameters (known as SR analysis). In SR analysis the objective was to estimate the surface eddy flux of a scalar from the scalar trace measured at one height. Most studies involving SR analysis mainly focused on estimation of sensible (or buoyant) heat flux, likely, for two reasons. Roughly, it allows for estimating the latent heat flux when the available net surface energy is measured or estimated (the well-known residual method; Brutsaert, 1982; Paw U et al., 2000). The SR equation for estimating the sensible heat flux (or any scalar) required calibration (Castellví, 2004; Castellví et al., 2002; Chen et al., 1997b; Katul et al., 1996; Shapland et al., 2012b; Snyder et al., 1996), but the air (or virtual) temperature measurements are simpler than for other scalars. Combining SR analysis, the one-dimensional turbulent diffusion equation and MOST, a modified SR analysis approach was derived which involved the friction velocity as input (Castellví, 2004). The latter performed similar to the eddy covariance (EC) method without requiring calibration (Castellví, 2004, 2013; Castellví & Snyder, 2009a, 2009b, 2010; Castellví et al., 2008, 2012; Suvočarev et al., 2014). The modified SR equation requires estimates of the friction velocity, the mean wind speed, and canopy parameters as well for input. Regardless, in comparison with other MOST-based methods, SR-based equations allow for

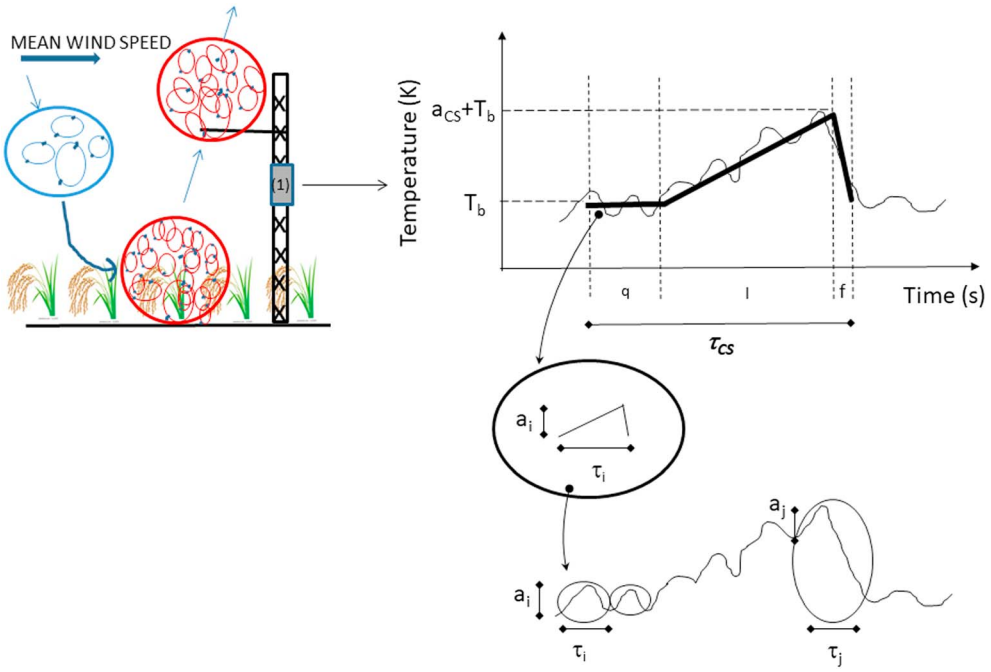

Figure 1. Surface renewal scheme for an unstable case. The earlier surface renewal analysis focused on the role of a coherent structure (top left) through determination of the ramp period (τ_{CS}) and amplitude (a_{CS}). After a quiescent period (q), the macroparcel of air (red) is heated during a period (l) until, by continuity, it is replaced (during a period f) by a cooler parcel (blue) coming from above with mean temperature T_b (top right). Temperature traces (thin solid line) recorded in a logger (1), show small fluctuations (eddies attached) embedded to the large coherent structure ramp-like shape. A small fluctuation follow a ramp-like shape where the period q can be neglected. Thus, the ramp periods (τ_i) can be estimated as the time between two consecutive valleys and the ramp amplitudes (a_i) as the temperature difference between a peak and the previous valley (bottom).

discriminating stable and unstable cases from measurements at one height and can be applied either in the roughness or inertial sublayers which allows minimizing fetch requirements (Castellví, 2012).

This study proposes an alternative SR analysis, which allows for estimating the sensible (or buoyant) heat flux and the friction velocity at neutral cases without involving MOST-based relationships. It is shown that either in the inertial or roughness sublayer, the SR-based method is exempt for calibration and the zero-plane displacement is the only canopy parameter involved. Furthermore, the latter may not be required depending on the surface and measurement height. The method requires as an input the mean wind speed and the air (or virtual) temperature sampled at high frequency (such as 8 or 10 Hz) for the surface heat flux and friction velocity estimation, and the canopy height because, in practice, the zero-plane displacement is estimated as a fraction of the canopy height. The performance is shown over a set of homogeneous and sparse canopies that may be considered representative of most agricultural crops.

2. Theory

2.1. Background

In SR analysis it is crucial to identify the coherent motion of a macroparcel of air (defined as a volume of air large enough to cover all the sources of scalar) from scalar concentration time series sampled at high frequency above the canopy. In SR analysis, it is assumed that most of the actual eddy flux is carried out by coherent structures (CS). For sensible heat flux, the following scheme (Figure 1) and assumptions were made (Paw U et al., 1995). A macroparcel of air, originally traveling at a given height, descends to the surface to remain in contact with the surface for a given period, τ_{CS}. While it remains in contact with the surface, no mass of air within the parcel is lost, and it is uniformly heated (or cooled) by a net amount of heat, $\rho C_p a_{CS}$ where ρ and C_p are the density and isobaric heat capacity of the air and a_{CS} is the temperature change during τ_{CS}. By continuity, the macroparcel of air ejects what represents an injection of heat into the atmospheric surface layer. Small eddies attached to the macroparcel of air (Figure 1) were presumed statistically independent of the

coherent structure. Therefore, while the main role of the coherent structure is to explain the surface eddy flux, the main role of eddies attached is to uniformly mix the concentration of scalar inside the macroparcel of air (Castellví & Snyder, 2009a; Katul et al., 1996). Ideally, a quasi-steady coherent motion would be featured in the temperature trace as a ramp-like pattern (typically termed the *signature* of a coherent structure) where the ramp is characterized by dimensions a_{CS} and τ_{CS} (termed ramp amplitude and period, respectively, Figure 1). In the actual time series (30 min), given the multitude of small fluctuations (smallest eddies) embedded in ramp-like events (coherent structures), the *analysis* consists of determining the mean ramp dimensions. Filtering tools and ramp models have been used for this purpose (Chen et al., 1997a; Katul et al., 1996; Paw U et al., 1995; Qiu et al., 1995; Shapland et al., 2012a; Van Atta, 1977), and, as an example, Figure 1 shows a ramp model which accounts for a quiescent period (q), a warming period (l), and a microfront period (f); thus, $\tau_{CS} = (q + l + f)$ (Chen et al., 1997a). For temperature, positive and negative values of a_{CS} discriminate unstable and stable cases, respectively. In SR analysis the surface eddy flux is explained by the frequency of injections of scalar concentration into the atmospheric surface layer. The sensible (or buoyant) heat flux (H) is expressed as, $H_{SR} = (\beta Z)\, \rho C_p \frac{a_{CS}}{\tau_{CS}}$ (Paw U et al., 1995) where β is a coefficient that corrects for the assumption that the parcel of air is uniformly heated, Z is the volume (V) of the parcel of air per unit surface area (S; thus, $Z = V/S$ is the measurement height because it is assumed that the parcel of air extends from the ground to the measurement height), and a_{CS} and τ_{CS} are the mean ramp dimensions determined from time series (half-hourly) of the temperature of the air (for sensible heat flux) or the virtual temperature of the air (for buoyant heat flux). When measurements are taken at the canopy top, the coefficient β is close to 0.5 to correct for the mean temperature gradient within the volume of the air parcel (Paw U et al., 1995). In the inertial sublayer, for unstable cases the coefficient β tends to be close to one (i.e., signatures of coherent motions are well defined indicating that the parcel of air is well mix), and under near-neutral and stable conditions β is close to 0.5 and smaller than 0.5, respectively, indicating that temperature fluctuations of the smallest eddies may be similar to the signature of the macroparcel of air (Castellví & Snyder, 2009a, 2009ab, 2009ac; Snyder et al., 1996). Therefore, in general, the coefficient β required calibration (against the EC method). Combining the turbulent diffusion equation and formulation based on MOST, the following approach was derived that model the parameter β half-hourly (Castellví, 2004), $\beta = \sqrt{\frac{K_h \tau_{CS}}{\pi Z^2}}$ where K_h is the eddy diffusivity for heat. The latter was parameterized as, $K_h = k\,(Z - d)\, u_* \phi_h^{-1}\left(\frac{Z-d}{L}\right)$ where k is the Von Kàrmàn constant, d is the zero-plane displacement, u_* is the friction velocity, L is the Obukhov length, and ϕ_h is the stability function for the heat transfer. The wind log-law was useful to estimate the friction velocity from low-frequency measurements of the wind speed. Therefore, canopy parameters were involved to determine H_{SR}.

2.2. The SR Analysis Based on Small Eddies

The following scheme and formulation is proposed to estimate the friction velocity and the surface heat (sensible or buoyant) flux:

1. Near the canopy, a macroparcel of air following a coherent motion cannot absorb all the momentum transferred to the ground. As a consequence, it breaks generating a population of small whirling parcels of air or eddies (in the following termed fluid elements) randomly distributed within the canopy (Zhu et al., 2007). During the time that a fluid element remains close (or in contact) to the viscous boundary layer adjacent to a source (exposure time), the mass of scalar and heat transfers through the interface and the fluid element increases (or decreases) its scalar concentration and temperature until it is randomly replaced by another fluid element (Danckwerts, 1951; Harriot, 1962).
2. By continuity, when a *fresh* macroparcel of air (i.e., originally traveling well above the surface) descends to renew the previous one, the abovementioned fluid elements will eject upward attached to the macroparcel of air. Thus, the ejection phase of the macroparcel of air represents an injection of a collection of fluid elements that broadly disperses into the atmospheric surface sublayer (Zhu et al., 2007) and the surface eddy flux can be determined integrating the eddy flux of fluid elements.
3. Inside the canopy, it will be assumed that the exposure time of a fluid element (τ) follows a probability distribution function, $\mathrm{PDF}_{(\tau)}$, described as (Bullin & Dukler, 1972; Seo & Lee, 1988)

$$\mathrm{PDF}_{(\tau)} = \frac{(\alpha+1)^{(\alpha+1)}}{\Gamma_{(\alpha+1)}} \frac{\tau^{\alpha}}{\overline{\tau}^{(\alpha+1)}} e^{-\left((\alpha+1)\frac{\tau}{\overline{\tau}}\right)}, \quad (1)$$

where Γ is the gamma function, α is a shape parameter, and $\bar{\tau}$ is the mean exposure time of fluid elements population. The exposure times in equation (1) can be estimated as the time difference between two consecutive peak and valley observed in fluctuations of the horizontal velocity in the vicinity of the interface (i.e., close to the surface where the renewal takes place; Haghighi & Or, 2013; Seo & Lee, 1988). The contribution of fluid elements with a short exposure time in equation (1) increased as the flow increased the Reynolds number (Seo & Lee, 1988). These authors suggested that the higher the turbulent intensity the smaller is the shape parameter α. On the other hand, taking measurements of the wind speed well above the surface (i.e., in the inertial sublayer), it was found that under near neutral conditions the shape parameter α, the mean wind speed (u) and the friction velocity were related as follows, $u_{*n} = \frac{0.3\ u}{(\alpha+1)}$ where subscript n denotes neutral atmospheric conditions (Haghighi & Or, 2013).

4. At a given reference height (Z) above the surface, time series of temperature of the air show small fluctuations embedded in large ramp-like events (Figure 1). It will be considered that a small fluctuation is the signature of a fluid element attached to the macroparcel of air and that the temperature change versus time follows a ramp-like shape characterized by a gradual increase of the temperature (warming phase) followed by a sudden drop in temperature (Figure 1). The latter indicates that this fluid element was replaced by another cooler fluid element. For signatures of fluid elements, given that its mass is small, it is presumed that the quiescent phase can be neglected. Therefore, because the temperature should be sampled at a very high frequency to clearly observe the peak and the sudden temperature drop, it is proposed that the signature of a fluid element can be estimated by the time difference (τ_i) observed between two consecutive valleys and by an amplitude (a_i) that is the temperature difference between the peak and the earlier valley (Figure 1). It is assumed that the PDF for the ramp period of fluid elements τ_i can be described by equation (1) and based on the relationship between turbulence intensity and the shape parameter α (Haghighi & Or, 2013; Seo & Lee, 1988), the following expression (derived in the Appendix) is proposed to estimate the friction velocity (half-hourly) under neutral conditions

$$u_{*n} = \begin{cases} \dfrac{k\,u}{\alpha} & \text{for } Z-d \geq (h_c-d)\left[\dfrac{3+\ln(\alpha)}{\ln(\alpha)}\right] \text{ (inertial)} \\ \dfrac{k\,u(h_c-d)}{\alpha\ (Z-\mathrm{d})}\left[\dfrac{3+\ln(\alpha_Z)}{\ln(\alpha_Z)}\right] & \text{for } Z-d < (h_c-d)\left[\dfrac{3+\ln(\alpha)}{\ln(\alpha)}\right] \text{ (roughness)} \end{cases}, \tag{2}$$

where h_c is the canopy height and α is the shape parameter determined from equation (1) sampling the temperature of the air at a moderate frequency, such as 8–10 Hz. To account for a given stability case, the friction velocity can be expressed as

$$u_* = u_{*n}\phi^{-1}_{m\left(\frac{Z-d}{L}\right)} \quad \text{where} \quad \phi_m = \begin{cases} \left(1-16\ \dfrac{Z-d}{L}\right)^{-1/4} & \text{for} \dfrac{Z-d}{L} \leq 0 \\ \left(1+5\ \dfrac{Z-d}{L}\right) & \text{for} \dfrac{Z-d}{L} \geq 0 \end{cases} \tag{3}$$

is the stability function for the transfer of momentum (Dyer, 1974).

5. Parameterizing the eddy diffusivity for heat (K_h) of the ith fluid element at the reference height (above the canopy) as, $K_{hi} = kl_{hi}w_i$ where l_{hi} and w_i denote mixing lengths for the transfer of heat and vertical wind velocity, respectively, and by assuming that the instantaneous local temperature gradient during the renewal phase is zero, the one-dimensional (vertical) turbulent diffusion equation allows estimating the mean (i.e., over the time duration of the fluid element, τ_i) local temperature gradient associated to the ith fluid element as; $\frac{\partial T_{i(z)}}{\partial z} = -\frac{a_i}{\sqrt{\pi\tau_i K_{hi}}}$ (Castellví, 2004, 2013). Thus, the flux-gradient relationship allows expressing the surface heat flux associated to the ith fluid element (H_i) as

$$H_i = \rho C_p \sqrt{\frac{K_{hi}}{\pi\ \tau_i}} a_i \tag{4}$$

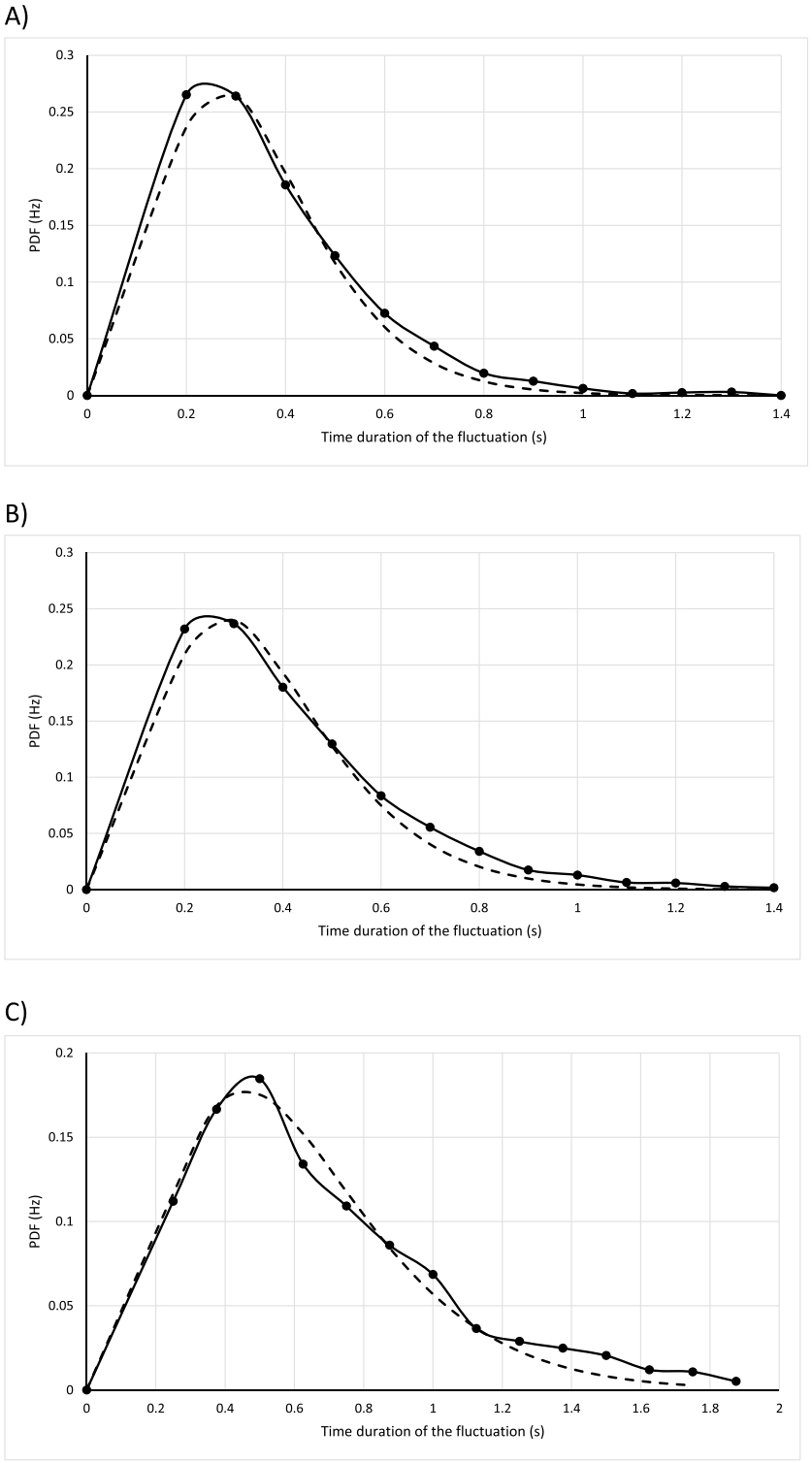

Figure 2. Actual (solid) and theoretical (dashed) $PDF_{(\tau)}$ for an air temperature time series (half an hour) over the rice field Y2 (0.2-m tall) for an (a) unstable case and (b) stable case, and (c) over the nectarine grove for an unstable case.

Table 1
Fitting the Theoretical to the Actual Probability Distribution Function for the Small Ramps Periods Observed in Three Half an Hour Temperature Time Series

Canopy	Z	h_c	N	$\overline{\tau}$	α	u	$u*$	H	s	R^2
Rice Y2	1.5	0.2	5213	0.345	3.45	1.18	0.14	15	0.98	0.99
Rice Y2	1.5	0.2	4860	0.37	3.03	1.35	0.18	−18	1.00	0.99
Nectarine	3.2	3.2	2901	0.62	3.00	1.16	0.40*	138	1.05	0.99

Note. $(^*)$ estimated as $u_* = 0.8\,\sigma_w$ where σ_w is the standard deviation of the vertical wind speed. An unstable and a stable case in the rice field Y2 and an unstable case in the nectarine grove. Z and h_c denote measurement and canopy heights (m), respectively, N is the number of fluid elements, $\overline{\tau}$ (s) is the mean ramp period, α is the shape parameter, u (m/s) is the mean wind speed, u_* (m/s) is the friction velocity, H (W/m^2) is sensible (or buoyant) heat flux, and s and R^2 are the slope and the coefficient of determination of the linear regression analysis, respectively.

6. By assuming that a fluctuation of the vertical wind speed (w') with respect to the mean vertical velocity (i.e., the associated to the macroparcel of air) is close to w_i and that small eddies are generated by shear (i.e., $\frac{1}{\tau_i}$ is expected to be related with $\frac{u'}{l_{mi}}$ where l_{mi} denotes mixing length for the transfer of momentum and u' a fluctuation of the horizontal mean wind speed), the diffusivity for the transfer of momentum of a fluid element is related with $k\,\tau_i(u'w')$. Consequently, through the turbulent Prandtl number P_{rt}, $\frac{K_{hi}}{\tau_i}$ in equation (4) is related with $\frac{k}{P_{rt}}\left(u'w'\right)$. Therefore, because $(u'w')$ is a summand in the calculation of the covariance $\overline{u'w'}$, which is close to u_*^2, $\frac{K_{hi}}{\tau_i}$ may be parameterized as, $\frac{K_{hi}}{\tau_i} = k f_i u_*^2$ where f_i is a weight (unknown). Here f_i is assumed to depend on the ratio $\frac{\tau_i}{\overline{\tau}}$ (i.e., higher weights are given to larger fluctuations) and on the stability conditions through the local stability function for the transfer of momentum. The following expression is proposed to estimate $\frac{K_{hi}}{\tau_i}$

$$\frac{K_{hi}}{\tau_i} = k\frac{\tau_i}{\tau}\phi^{-1}_{h\left(\frac{Z-d}{L}\right)}u_*^2 \quad \text{where} \quad \phi_h = \begin{cases} \phi^2_{m}\left(\dfrac{Z-d}{L}\right) & \text{for} \quad \left(\dfrac{Z-d}{L}\right) < 0 \\ \phi_{m}\left(\dfrac{Z-d}{L}\right) & \text{for} \quad \left(\dfrac{Z-d}{L}\right) \geq 0 \end{cases}. \tag{5}$$

7. Stationarity (half an hour) is in agreement with the derivation of stability functions for the transfer of momentum and heat. Thus, combining equations (2)–(5), the following expression is proposed to estimate the sensible (or buoyant) heat flux (H) on a half-hourly basis

$$H = \frac{Z_V}{N\,\overline{\tau}}\Sigma_{i=1}^{i=N}H_i\tau_i = Z_V\frac{\rho C_p\,\sqrt{\frac{k}{\pi}}\;\phi^{-1/2}_{h\left(\frac{Z-d}{L}\right)}\;\phi^{-1}_{m\left(\frac{Z-d}{L}\right)}}{N\,\overline{\tau}}\frac{k\,u}{\alpha}A\left(\Sigma_{i=1}^{i=N}\left(\frac{\tau_i}{\overline{\tau}}\right)^{1/2}\tau_i a_i\right), \tag{6}$$

where N is the total number of fluid elements (thus, $N\,\overline{\tau}$ equals 1,800 s), A depends on the reference height, $A = \begin{cases} 1 & \text{for } (Z-d) \geq (h_c-d)\left[\dfrac{3+\ln(\alpha)}{\ln(\alpha)}\right] \\ \dfrac{(h-d)}{(Z-d)}\left[\dfrac{3+\ln(\alpha_Z)}{\ln(\alpha_Z)}\right] & \text{for } (Z-d) < (h_c-d)\left[\dfrac{3+\ln(\alpha)}{\ln(\alpha)}\right] \end{cases}$, and Z_V (dimensionless) accounts for a representative volume (per unit surface area) containing all the fluid elements. It is proposed to parameterize Z_V as

$$Z_V = \begin{cases} (Z-d) & \text{homogeneous canopy} \\ (Z-d)f_c & \text{sparse canopy} \end{cases}, \tag{7}$$

where f_c is the fraction of ground cover. For orchards, where trees are planted in rows and the crowns along the row are close to each other, the following approach for f_c is suggested; $f_c = \frac{D_t}{D_r}$ where D_t and D_r denote distance between trunks in a row and between rows, respectively.

Table 2
Friction Velocity Estimates Versus Measured Using the EC Method for Each Crop, Stability Case, and All the Data

Sub-layer	Near-neutral									Unstable		
	equation (2)				equation (8)			equation (2)	equation (8)	equation (2)		
Inertial crop	*N*	*s*	int	R^2	*s*	int	R^2	RMSE		*N*	*s*	int
Grass	329	1.09	0.00	0.73	1.39	0.03	0.77	0.07	0.11	841	1.05	0.00
Rice Y1	1135	0.95	0.01	0.77	1.13	0.01	0.94	0.05	0.04	1005	0.77	0.01
Rice Y2	887	0.98	0.01	0.81	1.16	0.02	0.91	0.05	0.04	837	0.86	0.00
Roughness crop	equation (2)				equation (8)			equation (2)	equation (8)	equation (2)		
	N	*s*	int	R^2	*s*	int	R^2	RMSE		*N*	*s*	int
Rice Y1	305	0.96	0.00	0.83	—	—	—	0.04	—	1174	0.96	0.01
Rice Y2	507	0.87	0.03	0.76	—	—	—	0.05	—	882	0.86	0.00
Peach gr.	405	0.91	0.02	0.85	—	—	—	0.06	—	1369	0.65	0.03
Olive gr.	275	0.94	0.00	0.90	—	—	—	0.08	—	156	0.97	−0.02

Note. *N* is the number of samples, RMSE is the root-mean-square error (m/s), and s, int (m/s), and R^2 are the slope, the intercept, and the coefficient of determination of the linear regression analysis, respectively.

3. Materials and Methods

3.1. The Field Campaigns

A set of six experiments representative of most agricultural crops were used to test the performance of equations (3) and (6) versus the friction velocity and sensible heat flux, respectively, measured using the EC method. Experimental setup and main climate features are available in different papers. Crops representative of a homogeneous canopy were grass (Castellví & Snyder, 2010) and two rice fields (Castellví & Snyder, 2009b), and of a sparse canopy were groves of mature nectarine trees (Castellví et al., 2006), peach trees (Castellví & Snyder, 2009c), and olive trees (Castellví & Martínez-Cob, 2005). A summary of the campaigns is as follows.

3.1.1. Grass Field

The experiment was carried out at the UC West Side Research and Extension Center (Five Points, CA) from 22 August to 18 October 2007. The crop was maintained to 0.12-m tall, and the fetch, in practice, was considered unlimited. A three-dimensional (3-D) sonic anemometer (81000RE, RM Young, United States) operating at 10 Hz was deployed at a reference height of 1.17 m.

3.1.2. Rice Fields

The experiment was carried out simultaneously over two adjacent rice fields (Y1 and Y2) at Colusa (CA) that covered the full growing season in year 2007. Regardless of the field, the fetch was unlimited and the crop was growing from 0.1 up to 1.1 m. A 3-D sonic anemometer (81000RE, RM Young, USA) operating at 10 Hz was deployed in each rice field. The reference heights were 1.75 and 1.5 m in Y1 and Y2, respectively.

3.1.3. Nectarine Orchard

This experiment was carried out at Atalia (Portugal) from 16 to 23 July 1989. The fetch was unlimited, the trees were 3.2 m tall, and the distance between trunks in a row was 3.5 and 5 m between rows. A 1-D sonic anemometer (CA27, Campbell Sci.) and a thermocouple operating at 10 Hz were deployed at a reference height of 3.5 m to determine the sensible heat which was directly stored in the data logger (raw data was not stored). Thermocouples operating at 8 Hz were deployed inside the canopy at 0.8, 1.4, 2.0, 2.6, and 3.2 m above the ground (raw data was stored). The horizontal mean wind speed was available at 3.5 m.

3.1.4. Peach Orchard

This experiment was carried out at the Kearney Research and Extension Center (Parlier, CA) from 2 August to 16 October 2007. The fetch was 240 m, the trees were 4.0 m tall, and the distance between trunks in a row was 2 and 5 m between rows. A 3-D sonic anemometer (81000RE, RM Young, United States) operating at 10 Hz was deployed at a reference height of 5.5 m.

3.1.5. Olive Orchard

This experiment was carried out at the Ebro river basin (Zaragoza, Spain). The fetch was unlimited, the trees were 3.5 m tall, and the distance between trunks in a row was 3 and 6 m between the rows. A 3-D sonic

Table 2 *(continued)*

Sub-layer	Unstable						Stable					
	equation (2)	equation (3)			equation (2)	equation (3)	equation (2)				equation (3)	
Inertial crop	R^2	s	int	R^2	RMSEe		N	s	int	R^2	s	int
Grass	0.74	1.07	0.00	0.76	0.05	0.06	1726	1.03	0.06	0.81	1.07	0.02
Rice Y1	0.75	0.80	0.05	0.63	0.05	0.06	1091	1.06	0.01	0.85	1.04	0.02
Rice Y2	0.77	0.86	0.03	0.76	0.05	0.04	763	1.04	0.02	0.88	1.07	−0.01
Roughness crop	equation (2)	equation (3)			equation (2)	equation (3)	equation (2)				equation (3)	
	R^2	s	int	R^2	RMSE		N	s	int	R^2	s	int
Rice Y1	0.75	0.96	0.00	0.79	0.06	0.05	397	0.87	0.04	0.73	0.80	0.01
Rice Y2	0.79	0.85	0.02	0.78	0.05	0.04	476	1.02	0.03	0.78	1.01	0.01
Peach gr.	0.74	0.86	0.03	0.74	0.08	0.07	1523	0.77	0.07	0.68	0.74	0.01
Olive gr.	0.90	0.99	0.02	0.91	0.08	0.07	201	0.71	0.09	0.78	0.81	0.02

anemometer (CSAT3, Campbell Sci.) and a thermocouple operating at 10 Hz were deployed at a reference height of 5.1 m from 1to 10 April 1995.

3.2. Determining the Shape Parameter α, the Friction Velocity, and the Sensible Heat Flux. Performance Evaluation

To determine the shape parameter α, equation (1) was fit to the actual PDF using the Brent's root-finding algorithm method to minimize the root mean square error (Brent, 1973; Nash, 1990). The zero-plane displacement was estimated as $d = 2/3h_c$, where h_c is the canopy height which is a representative value for most crops (Brutsaert, 1982). Therefore, the remaining parameter required to solve equations (3) and (6) is the stability parameter. Thus, the Obukhov length, u_*, H and the stability parameter were calculated iteratively. Starting at neutral conditions ($L = \infty$), equations (3) and (6) provide a rough estimate for u_* and H, respectively, which allows for determining a first estimation for the stability parameter. The latter was used in equations (3) and (6) to obtain the first estimate for u_* and H. An unknown extrarelationship is required to establish a set of equations allowing for an objective criteria for convergence. Therefore, regardless of the stability case, one iteration was implemented to calculate u_* and H.

The friction velocity and surface heat flux estimates were compared versus the values determined using the EC method (reference) calculating the slope, the intercept and the coefficient of determination (R^2) of the linear regression analysis, and the root-mean-square error (RMSE). For neutral stability cases, the friction velocity determined using the wind log-law valid in the inertial sublayer for a homogeneous surface was included in the comparison

$$u_* = \frac{k\ u}{\ln\left(\frac{Z-d}{z_{0m}}\right)} \quad \text{for} \quad Z - d \geq (h_c - d)\left[\frac{3 + \ln\alpha}{\ln\alpha}\right], \tag{8}$$

where z_{0m}, estimated as $z_{0m} = 0.12h_c$, is the roughness length for momentum (Brutsaert, 1982) and the bottom of the inertial sublayer was estimated from equation (A12).

At the nectarine grove, the EC friction velocity was not measured (i.e., a 1-D sonic anemometer was available) and the sensible heat flux was estimated assuming that the shape parameter α determined at the canopy top remained fairly constant versus height in the roughness sublayer because the horizontal mean wind speed was not available at the canopy top.

4. Results

4.1. The PDF for the Duration of Air Temperature Fluctuations

Regardless of the crop, reference height and stability case, in general the actual and theoretical PDF were similar as shown in Figure 2 for a sample obtained under unstable (Figure 2a) and stable at night

Table 2 *(continued)*

Sub-layer	Stable			All data								
	equation (3)	equation (2)	equation (3)	equation (2)				equation (3)			equation (2)	equation (3)
Inertial crop	R^2	RMSE		N	s	int	R^2	s	int	R^2	RMSE	
Grass	0.85	0.08	0.05	2567	0.98	0.05	0.75	1.04	0.02	0.82	0.07	0.06
Rice Y1	0.89	0.06	0.05	2096	0.96	0.01	0.78	0.96	0.01	0.77	0.05	0.05
Rice Y2	0.91	0.05	0.04	1600	0.98	0.00	0.78	0.99	0.00	0.85	0.05	0.04
Roughness crop	equation (3)	equation (2)	equation (3)	equaton (2)				equation (3)			equation (2)	equation (3)
	R^2	RMSE		N	s	int	R^2	s	int	R^2	RMSE	
Rice Y1	0.77	0.05	0.04	1571	0.91	0.02	0.74	0.94	0.00	0.80	0.06	0.05
Rice Y2	0.78	0.06	0.05	1358	0.87	0.02	0.67	0.91	0.02	0.77	0.06	0.05
Peach gr.	0.74	0.09	0.08	2892	0.67	0.02	0.64	0.84	0.02	0.76	0.08	0.07
Olive gr.	0.84	0.08	0.07	357	0.84	0.05	0.89	0.99	0.00	0.92	0.08	0.07

(Figure 2b) conditions over the rice field Y2 (0.2-m tall) and over nectarines (reference height was the canopy top) for an unstable case (Figure 2c). For the three samples shown in Figure 2, Table 1 shows the measured mean wind speed, the friction velocity and the sensible (or buoyant) heat flux, the calculated number of fluid elements and mean time duration, and the slope and coefficient of determination of the linear regression analysis obtained to force the best fitting of equation (1) to the actual PDF for calculating the shape parameter α. For the nectarine grove, the friction velocity was estimated as, $u_* = 0.8\ \sigma_w$ where σ_w is the standard deviation of the vertical wind speed (Castellví et al., 2006; Leclerc & Foken, 2014). Regardless of the crop, measurement height and stability conditions, both the slope and coefficient R^2 of the linear regression analysis were, in practice for most samples, one (as shown in Table 1). Under stable cases and calm conditions it may occur that the duration of the fluctuations fall within a narrow range (i.e., within two or three consecutive bins where the bin width was $2/f$ where f is the frequency of measurement) and, therefore, the shape parameter α was high. Though these samples clearly appeared as outliers (i.e., the friction velocity is close to zero), they were also included in the data sets. Regardless, in general, the spectrum of small eddies ejected upward (i.e., attached to the macroparcel of air) was well described by equation (1). The latter is crucial because equation (1) is the basis of the SR analysis based on small eddies.

4.2. The Friction Velocity

In the following, because the zero-plane displacement was estimated, near-neutral cases were considered to have a stability parameter in the range (taken as a rule of thumb) $0.1 \leq \frac{Z-d}{L} \leq 0.1$. For all crops (excluding the nectarines orchard), the Table 2 shows the results of the linear regression analysis and the RMSE comparing the performance of equations (2) and (3) to estimate the friction velocity versus the measured (u_{*EC}) for different stability cases. For near neutral conditions the Table 2 includes the performance of equation (8) when the measurements were taken in the inertial sublayer. For unstable and stable cases the performance of equation (2) was included to show the change of the estimates after one iteration.

4.2.1. The Friction Velocity and the Shape Parameter α Above the Canopy Under Near-Neutral Conditions

4.2.1.1. Measurements Made in the Inertial Sublayer

The comparison of equations (2) and (8) versus u_{*EC} is shown in Figures 3 for each crop. The intercepts of the linear regression analysis comparing equations (2) and (8) versus u_{*EC} were near to zero (Table 2). Regardless of the crop, the slopes obtained using equation (2) were closer to one than using equation (8). For grass, equations (2) and (8) overestimated friction velocity 9% and 39%, respectively, compared to the EC reference values. Figure 3a shows a set of friction velocity estimates that clearly underestimated the determined using the EC method. These samples were collected under calm conditions about 2 hr after midday when the surface layer became stable. Advection of warm air at the top of the atmospheric boundary layer around midday is a pattern of the climate at this site during summer (Castellví &

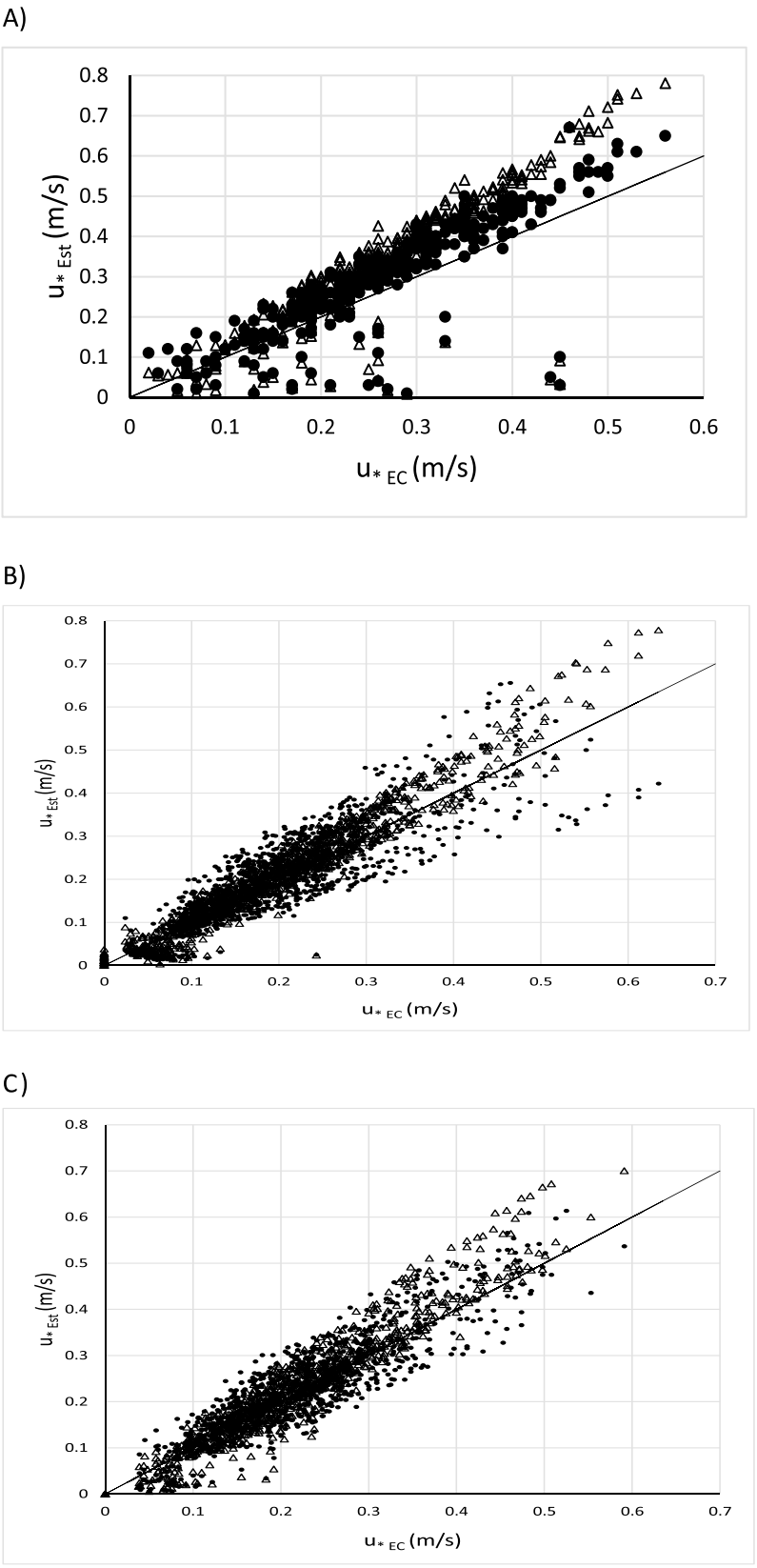

Figure 3. Friction velocity estimates near neutral conditions, equation (2) (dots) and equation (8) (triangles) versus u_{*EC} for all the data gathered in the inertial sublayer over (a) grass, (b) rice Y1, and (c) rice Y2.

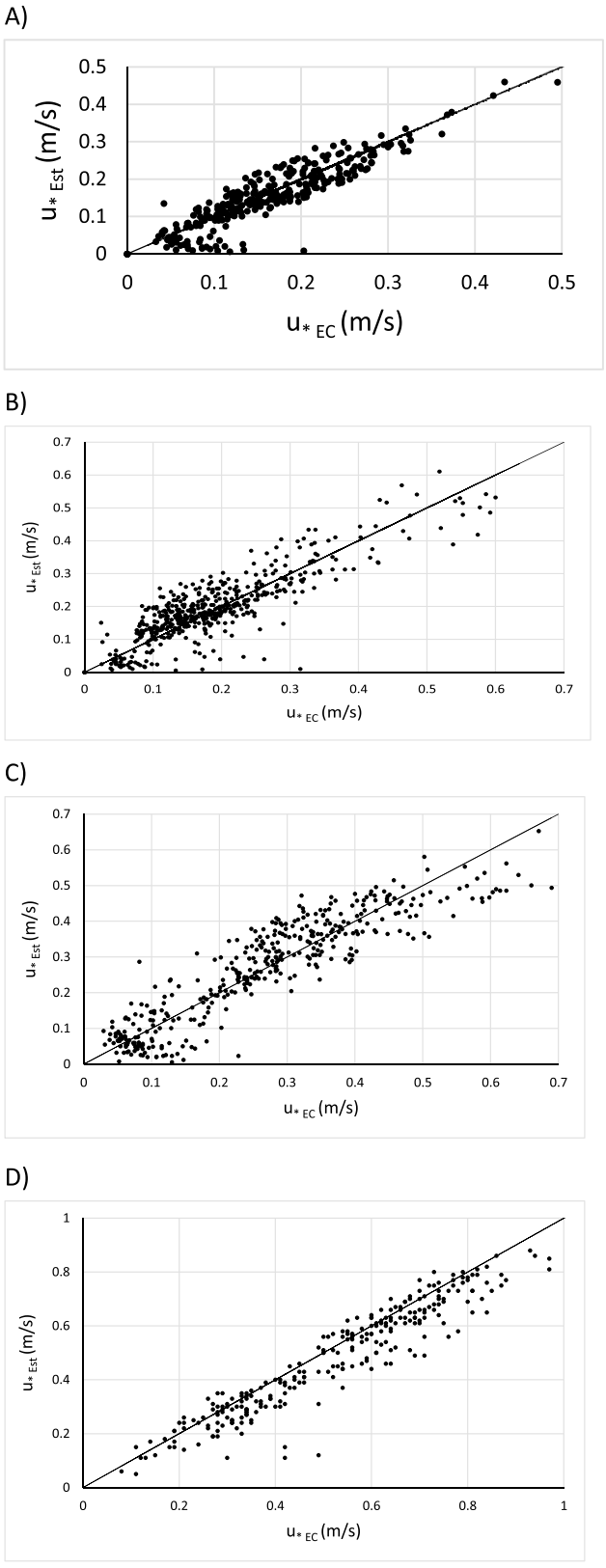

Figure 4. Friction velocity estimates using equation (2) versus u_{*EC} for all the data gathered in the roughness sublayer near neutral conditions over (a) rice Y1, (b) rice Y2, (c) peach grove, and (d) olive grove.

Snyder, 2010). For the rice fields, the friction velocity estimates were scattered along the 1:1 line (Figures 3b and 3c). Regardless of the crop, equation (8) was better correlated with u_{*EC} than with equation (2). The results shown in Table 2 and Figures 3 were similar for shorter data sets ($-0.05 \leq \frac{Z-d}{L} \leq 0.05$) that only included samples observed during the transition from negative to positive H_{EC} (and vice versa). For the latter data sets, while the coefficient R^2 obtained using equation (8) was the same, the R^2 obtained using equation (2) was improved slightly (though still smaller than the R^2 using equation (8)). The RMSE using equations (2) and (8) were similar for the rice fields (0.05 and 0.04 m/s, respectively), but over grass the RMSE using equation (2) was smaller than using equation (8). Equation (2) is not dependent on canopy parameters when the measurements are made during near-neutral conditions in the inertial sublayer. Therefore, for grass, the overestimation shown in Table 2 using the wind log-law may suggest that the standard parameterization of the canopy parameters was not reliable. By assuming that the estimation of the zero-plane displacement was reliable, the roughness length required in equation (8) to match the slope of equation (2) was $z_{0m} = 0.1h_c$ and to match u_{*EC}, $z_{0m} = 0.08h_c$. The performance of equation (2) versus u_{*EC} suggests that in the framework of MOST, the shape parameter α can be parameterized as, $\alpha = \ln\left(\frac{Z-d}{z_{0m}}\right)$, which indicates that α encapsulates crucial information of the surface roughness elements (the place where most fluid elements originated) and it increases with height. The latter, though measurements were made over growing crops (i.e., measurement height above the canopy was changing), could not be directly shown because measurements of the temperature of the air and the mean wind speed at several heights above the canopy were not available.

4.2.1.2. Measurements Taken Above the Canopy in the Roughness Sublayer

The performance of equation (2) is shown for each crop in Figures 4. Regardless of the crop, when equation (2) predicted friction velocities in the range 0 m/s $< u_{*Est} \leq$ 0.1 m/s, the estimates obtained for a few samples differed by more than 0.1 m/s from the reference (Figure 4) because the shape parameter α was large. The latter is a consequence of the fact that the time duration of the fluctuations fall within two or three bins of the PDF. Though these few samples slightly distorted the results of the linear regression analysis, all the data shown in Figures 4 was included in the results shown in Table 2. In general, the Figures 4 show that the estimates scattered along the 1:1 line, the slopes and intercepts were close to one and zero, respectively, and the coefficients of determination were in the range $0.76 \leq R^2 \leq 0.90$ (Table 2). Thus, equation (2) performed reliably given that the RMSE was in the range 0.04 m/s $\leq$ RMSE $\leq$ 0.08 m/s. The variability of the shape parameter α versus the canopy height (normalized by the reference height) for all crops is shown in Figure 5, which suggests that an intermediate value for α was around 3.25 near neutral conditions. On the other hand, though the αprofile above the canopy in the roughness sublayer was not available, the close performance of equation (2) versus u_{*EC} for the rice fields allow suggesting that the assumption made on that the shape parameter α remains fairly constant versus height

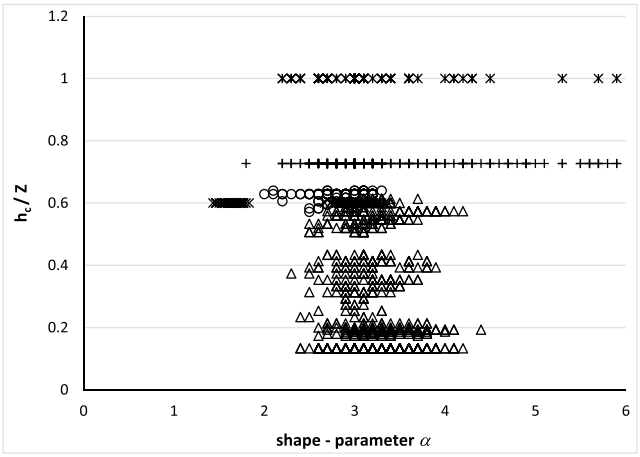

Figure 5. Shape parameter α determined above the canopy near neutral conditions vs the canopy height normalized by the reference height over the rice field Y1 (circle), rice field Y2 (triangle), and peach (cross), nectarine (star), and olive (x) groves.

above the canopy in the roughness sublayer (see Appendix) was, in practice, reliable.

4.2.2. The Shape Parameter α Inside the Canopy at Neutral Conditions

For the nectarine grove, the mean α profile inside the canopy shows that α consistently decayed (from the canopy top) until a height that can be presumed close to the zero-plane displacement (Figure 6). After reaching the consistent decay in the crown, the α profile appeared unpredictable (i.e., difficult to explain) because most samples showed a local maximum around half the canopy height (not shown). Such results suggest that below d, the shape parameter α becomes decoupled from the crown. The shear-scale (L_s), defined as $L_s = \frac{u_{z=h_c}}{\frac{du}{dz}}$, is a crucial length in the roughness sublayer (Raupach et al., 1996), which can be related with the shape parameter α determined at the canopy top (see Appendix). The latter relationship assumed that from the zero-plane displacement up to the canopy top, α tends to increase exponentially with height (equation (A10)). The exponential increase of α with height above the zero-plane displacement inside the canopy was not clearly shown in Figure 6 because more measurement levels were required. However, indirectly, based on the results shown in Figure 4, it can be stated that the L_s parameterization using α at the canopy top is, in practice, reliable. Partly (through equation (A10)), again (i.e., as for the inertial sublayer), α can be parameterized involving the leaf area index and drag coefficients (leaf and soil) (Graefe, 2004).

4.2.3. The Shape Parameter α Above the Canopy and the Friction Velocity Under Stable and Unstable Conditions

The shape parameter α is an eddy spectrum coefficient, and consequently, one expects a relationship between α and the stability parameter. For all the data collected over the rice field Y2 (one plot for measurements taken in the inertial sublayer and another for the roughness sublayer) and the peach grove, Figures 7 show the shape parameter α versus the stability parameter. These two crops were selected as representative of a homogeneous and a sparse canopy, respectively. The Figures 7 clearly show that α depends on the stability conditions and that regardless of the measurement height, most data follow the relationship $\alpha = p_1 \phi_{m\left(\frac{z-d}{L}\right)}^{-p_2}$ where p_1 and p_2 are empirical coefficients. For the rice field Y2, p_1=3.25 and p_2=2/5 (regardless of the measurement height and stability case). For the peach grove, p_1=3.5 and p_2=2/5 for unstable cases and p_1=3.0 and p_2=1/4 for stable cases. Thus, through α, the actual stability parameter is partly accounted in equation (2) or when a first approximation of the actual friction velocity (i.e., setting $L = \infty$ in equation (3)) is calculated to solve the friction velocity and the heat flux simultaneously.

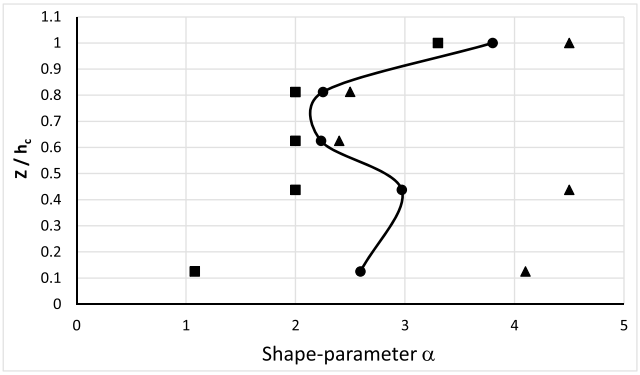

Figure 6. Mean α profile (solid line) inside the canopy of nectarine trees near-neutral conditions. For each measurement height (normalized by the canopy height), the mean α value (circle) is shown within the maximum (triangle) and the minimum (square) values.

For each crop and for all the data, Figure 8 compares the computed friction velocity (equation (3)) with the measured friction velocity from the EC (i.e. the reference, u_{*EC}). Regardless of the crop, the estimates scattered along the reference and, in general, the worst agreement was obtained for $u_{*EC} \leq 0.1$ m/s. The latter were observed under calm conditions ($u \leq 0.5$ m/s) during the night and at 2–3 hr after noon for clear sky days during the transition unstable stable case.

4.2.3.1. Measurements in the Inertial Sublayer

For unstable cases, in general, equations (2) and (3) performed close (Table 2). Thus, the inherent α dependency on the stability parameter (Figure 7) was sufficient to obtain estimates close to u_{*EC}. Therefore, the friction velocity may be estimated without involving canopy parameters and without the need to estimate the sensible heat flux. For stable cases, with respect to equation (2), equation (3) mainly

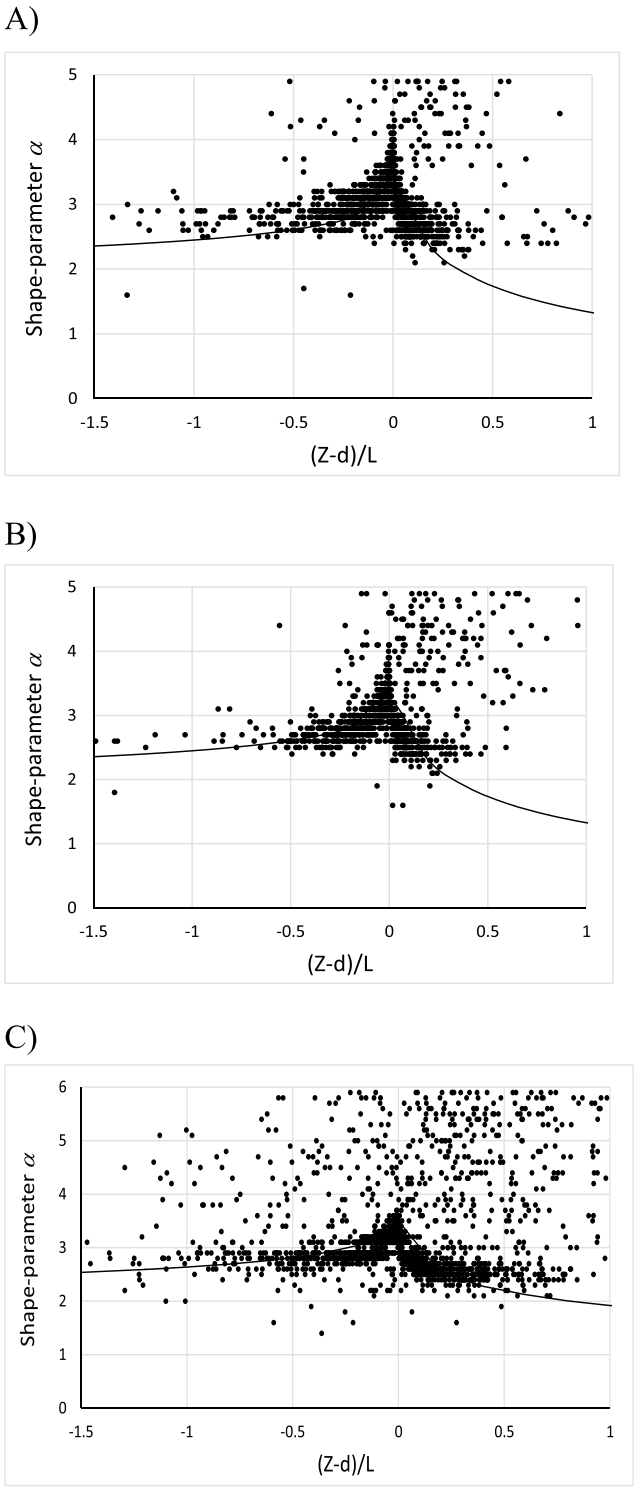

Figure 7. Shape parameter α versus the stability parameter for all the data collected over the rice field Y2 in (a) the inertial sublayer and (b) the roughness sublayer, and (c) over the peach grove. Solid lines show the relationship $\alpha = p_1\ \phi_{m\left(\frac{Z-d}{L}\right)}^{-p_2}$.

improved the results of the linear regression analysis for the coefficient of determination, $0.81 \leq R^2 \leq 0.88$ (equation (2)) versus $0.85 \leq R^2 \leq 0.91$ (equation (3)), and slightly the RMSE, 0.04 m/s ≤ RMSE ≤ 0.05 m/s (equation (3)) versus 0.05 m/s ≤ RMSE ≤ 0.08 m/s (equation (2)). For all the data, in general, equation (3) tended to compare slightly better to the measured reference than equation (2).

4.2.3.2. Measurements in the Roughness Sublayer

For unstable cases the Table 2 shows that with respect to equation (2), equation (3) improved slightly the slope for the rice field Y2 and the coefficient of determination for the peach grove. In general, the RMSE was in the range 0.04 m/s ≤ RMSE ≤ 0.07 m/s (equation (3)) while using equation (2) was 0.05 m/s ≤ RMSE ≤ 0.08 m/s. For simplicity, when the canopy height remains constant it may be suggested to estimate the friction velocity from equation (2) deploying the instrumentation close to the canopy top because the zero-plane displacement is not involved. For stable cases, with respect to equation (2), equation (3) improved the intercept, 0.01 m/s ≤ int ≤ 0.02 m/s (equation (3)) versus 0.03 m/s ≤ int ≤ 0.09 m/s (equation (2)), and the coefficient of determination, $0.74 \leq R^2 \leq 0.84$ (equation (3)) versus $0.68 \leq R^2 \leq 0.78$ (equation (2)), of the linear regression analysis and slightly the RMSE, 0.04 m/s ≤ RMSE ≤ 0.08 m/s (equation (3)) versus 0.05 m/s ≤ RMSE ≤ 0.09 m/s (equation (2)).

For all the data, equation (3) consistently compared slightly better to the measured reference than equation (2). In particular, equation (3) was closer than equation (2) to u_{*EC} for sparse canopies, which, partly, may be explained because α versus the stability parameter showed higher scatter for a sparse than for a homogeneous canopy (Figures 7).

The turbulent Prandtl number, *Pr*, was involved in equation (3) because the friction velocity is estimated using time series of temperature (see section A4. in the appendix). Indirectly, the good performance obtained using equation (3) (Table 2) supports the formal *Pr* dependency introduced in equation (A4). Furthermore, considering that the following relationship holds between the friction velocity and the mean wind speed at the canopy top (u_h) near-neutral conditions, $u_h \approx p_3\ u_*$ where p_3 is an empirical coefficient of about 3.5 (Graefe, 2004), combining the latter with equation (A4) allows approaching the Von Kàrmàn constant to $k \approx \frac{\alpha}{3.5} P_r$. This approach is rather consistent with the consensus that near neutral conditions at the canopy top *Pr* is about 0.5 and that the shape parameter alpha is about 3.25 (intermediate value in Figure 7c).

4.3. Estimation of the Sensible Heat Flux

For each crop, Table 3 shows the results of the linear regression analysis and the RMSE obtained from comparing the surface heat flux estimates ($H_{Eq.\ 6}$) to the measured reference (H_{EC}) in the inertial and roughness sublayers for unstable and stable cases and for all data. Table 3 includes initial ($H_{\_0\_Eq.\ 6}$) and first ($H_{\_1\_Eq.\ 6}$) iteration of $H_{Eq.\ 6}$. For each crop, the Figures 9 shows $H_{\_1\_Eq.\ 6}$ versus H_{EC} for all the data.

Table 3 shows, excluding the experiment conducted in the nectarine grove where the measurements were made at the canopy top, significant changes in the slope of the linear regression analysis between $H_{\_0\_Eq.\ 6}$ and $H_{\_1\_Eq.\ 6}$. For unstable cases, the changes in the slope (%), with respect $H_{\_0\_Eq.\ 6}$, varied between 44% (grass) and 132% (rice Y2) for measurements made in the inertial sublayer and between 33% (olive grove) and

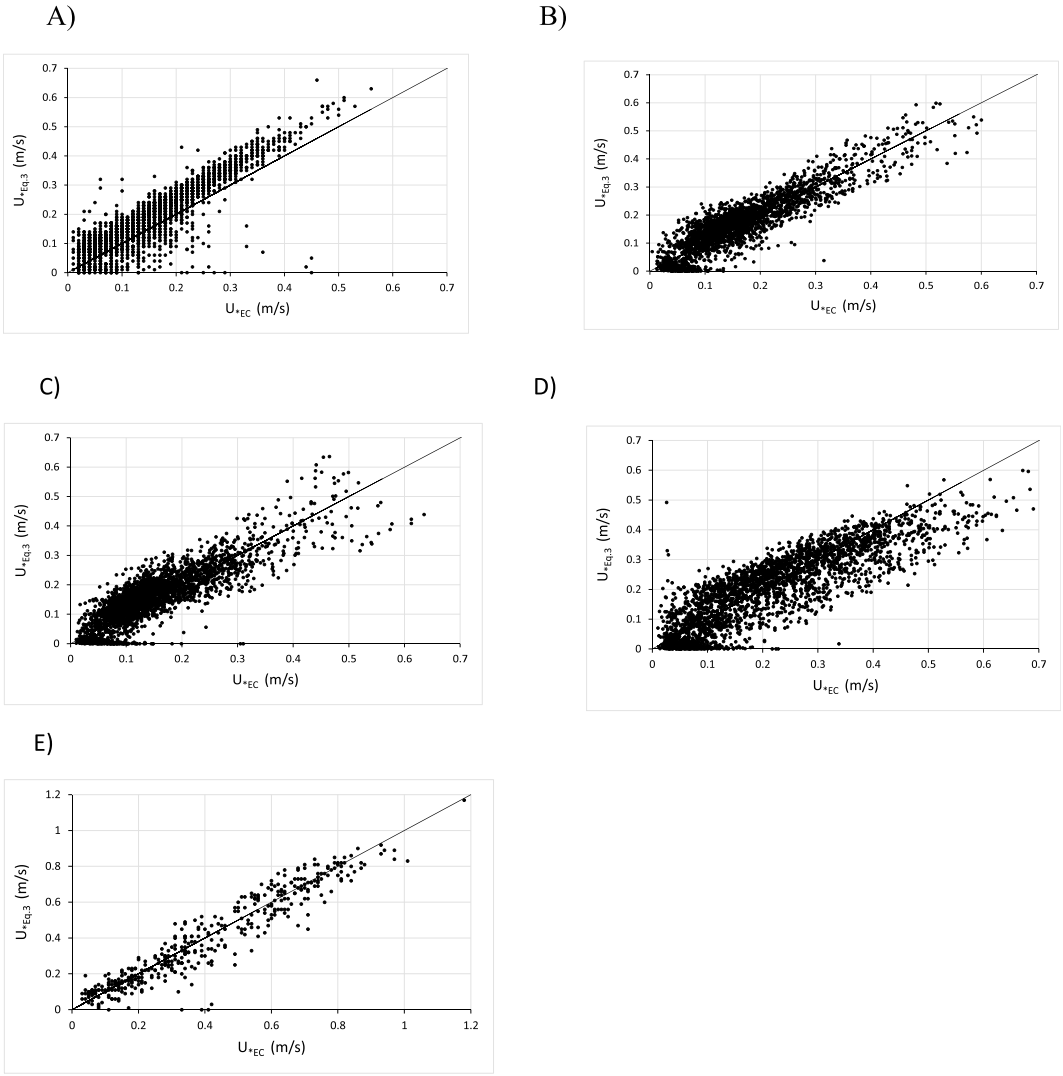

Figure 8. Friction velocity estimates versus u_{*EC} for all the data collected over (a) grass, (b) rice field Y1, (c) rice field Y2, (d) peach grove, and (e) olives grove.

Table 3
Surface Heat Flux Estimates Versus Measured Using the EC Method for Each Crop, Stability Case and All the Data

Sub-layer	Unstable									Stable				
	H_0_Est				H_1_Est			H_0_Est	H_1_Est	H_0_Est				H_1_Est
Inertial crop	N	s	int	R^2	s	int	R^2	Rmse		N	s	int	R^2	s
Grass	841	0.65	4	0.41	0.94	2	0.60	22	19	1726	1.32	−8	0.85	1.13
Rice Y1	1005	0.54	3	0.60	1.20	−1	0.88	23	17	1091	1.80	−1	0.85	1.27
Rice Y2	837	0.37	8	0.38	0.86	3	0.76	27	14	763	1.43	−4	0.75	1.22
Roughness														
Rice Y1	1174	0.50	1	0.66	1.13	−1	0.89	35	16	397	1.22	−7	0.84	0.90
Rice Y2	882	0.34	4	0.76	0.76	3	0.65	35	21	476	1.11	−4	0.78	1.00
Peach gr.	1369	0.49	7	0.60	0.87	15	0.81	51	29	1523	1.37	−16	0.62	0.93
Olive gr.	156	0.60	28	0.61	0.80	30	0.74	66	49	201	1.01	−6	0.58	0.93
Nectarine gr.	89	1.22	−26	0.84	1.24	−23	0.85	41	40	68	0.58	−3	0.52	0.60

Note. H_0_Est and H_1_Est are calculation of equation (6) setting neutral conditions and using the first estimation of the stability parameter, respectively, N is number of samples, RMSE is the root-mean-square error (W/m^2), and s, int (W/m^2), and R^2 are the slope, the intercept, and the coefficient of determination of the linear regression analysis, respectively.

equation (6). It would be desirable to state an objective criterion of convergence. The latter requires a consensus to establish a relationship between the shape parameter α and the stability parameter, such as $\alpha = p_1 \phi_{m\left(\frac{z-d}{L}\right)}^{-p_2}$. However, the close performance between $H_{\_1\_Eq.\ 6}$ and H_{EC} allows stating that one iteration provides reliable H estimates. The best flux estimates performance (i.e., closest to the reference) for each experiment were obtained with one iteration (not shown). The recommendation of implementing one iteration is not based on a rule of thumb. For field applications, it may be of interest to mention (not shown) that when instrumentation is deployed well above the ground over a short canopy, such as for the grass experiment, the zero-plane displacement can be neglected. Thus, for this particular case the friction velocity and the sensible heat flux can be estimated from the mean wind speed and the temperature trace.

Regardless of the experiment, the performance of $H_{\_1\_Eq.\ 6}$ was similar (RMSE within 5%) to the obtained using the earlier SR equation described in Castellví (2004; SR_{C_04}). When the instrumentation was deployed in the roughness sublayer, SR_{C_04} was applied by implementing semiempirical relationships for estimating canopy parameters and the roughness sublayer depth (Graefe, 2004). Thus, extra measurements or estimates were involved such as the horizontal wind speed measured at high frequency, leaf area index, plant area index, and the drag coefficient at leaf scale (Castellví et al., 2006; Castellví & Martínez-Cob, 2005; Castellví & Snyder, 2009b, 2009c). In the inertial sublayer the main difference (in terms of input requirements) is that the roughness length for momentum was not involved in equation (6) (Castellví & Snyder, 2010). Therefore, equation (6) is suitable for field applications and applied research, such as estimation of water requirements in hourly or daily basis using the residual method (shown in previous research), and offers tremendous advantages over SR_{C_04} and over SR approaches requiring calibration.

In EBEX-2000 project (Foken & Oncley, 1995) one of the studies performed consisted on the comparison of u_{EC} and H_{EC} determined using different postfield data processing protocols and 3-D sonic anemometer brands (Mauder et al., 2007). The EC instrumentation operated at 20 Hz, and it was deployed in the inertial sublayer. The comparisons were performed using samples that passed a quality control, including thresholds to assure well developed turbulence. For u_{EC} it was shown that the slopes of the linear regression analysis and the root-mean-square difference (RMSD) obtained taking as a reference the postprocessing protocol (Mauder & Foken, 2004) and CSAT3 were in the range, $0.97 \le s \le 1.10$ and 0.02 m/s $\le$ RMSD $\le$ 0.04 W/m^2, respectively. For H_{EC}, $0.83 \le s \le 1.22$ and 6.1 W/m^2 $\le$ RMSD $\le$ 12.8 W/m^2, respectively. The intercepts and coefficients of determination of the linear regression analysis were, in practice, zero and one, respectively. The reported EBEX-2000's comparisons for slopes and RMSD suggest that equations (3) and (6) may be considered to fill gaps in half-hourly EC series because all shortcomings inherent in the sonic anemometer are avoided, such as data compromised by turbulent flow distortions due to instrument and tower mounts in a given wind sector.

Table 3 *(continued)*

Sub-layer	Stable				All data								
	$H_{\_1\_Est}$		$H_{\_0\_Est}$	$H_{\_1\_Est}$	$H_{\_0\_Est}$				$H_{\_1\_Est}$			$H_{\_0\_Est}$	$H_{\_1\_Est}$
Inertial crop	int	R^2	Rmse		N	s	int	R^2	s	int	R^2	Rmse	
Grass	−3	0.85	20	12	2567	1.09	−12	0.84	1.12	−2	0.89	21	15
Rice Y1	2	0.86	10	10	2096	0.94	−12	0.76	1.18	0	0.93	23	14
Rice Y2	0	0.73	17	12	1600	0.77	−11	0.73	1.04	−2	0.89	23	13
Roughness													
Rice Y1	−2	0.87	16	7	1571	0.70	−13	0.81	1.10	1	0.94	29	13
Rice Y2	−2	0.80	13	10	1358	0.58	−9	0.71	0.81	−1	0.86	25	15
Peach gr.	−4	0.72	37	14	2892	0.78	−23	0.74	0.98	2	0.90	44	22
Olive gr.	0	0.50	20	21	357	0.76	−4	0.82	0.93	5	0.88	47	37
Nectarine gr.	−2	0.53	10	10	167	1.06	−5	0.87	1.08	−3	0.88	32	30

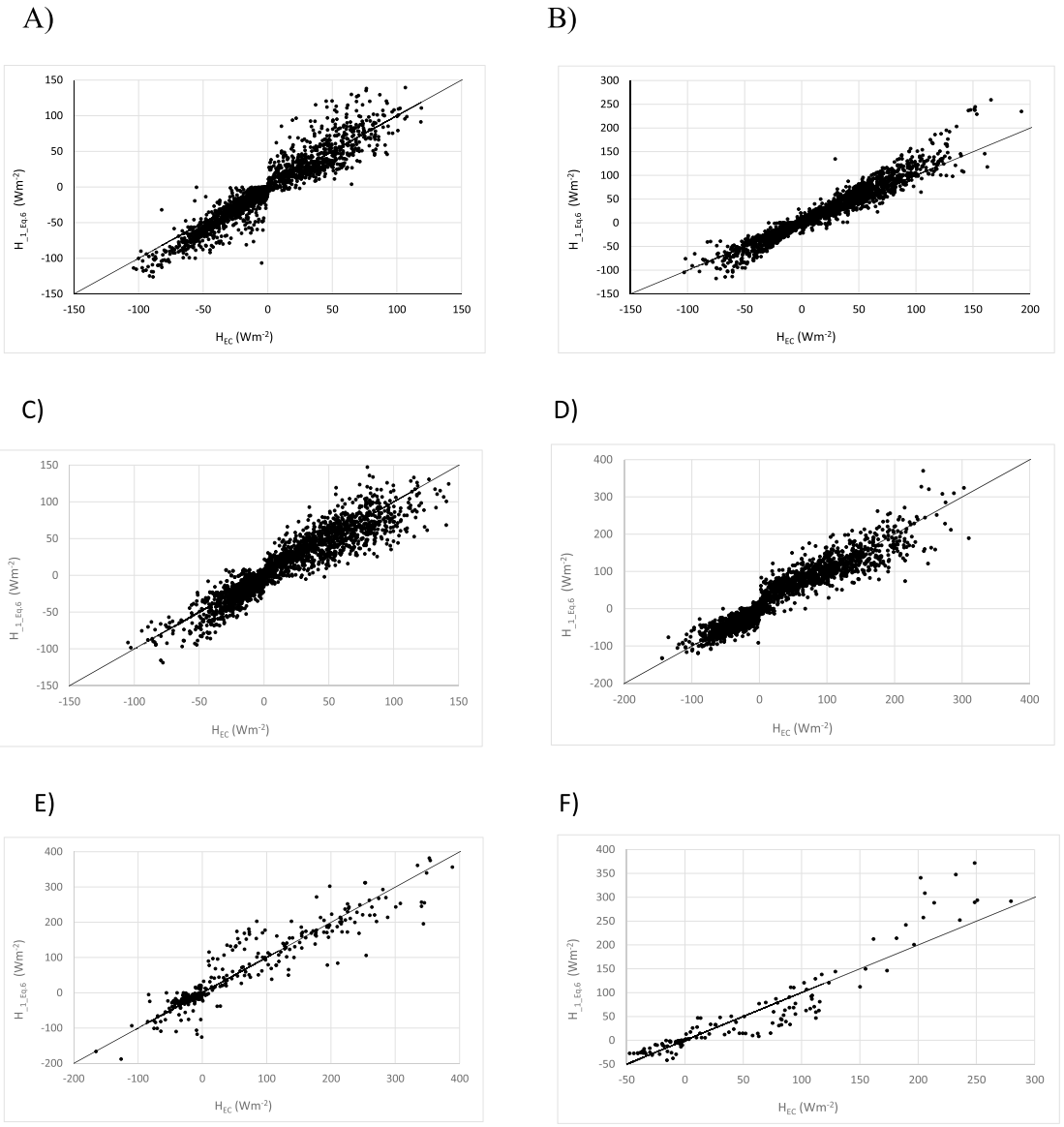

Figure 9. Buoyant heat flux estimates over (a) grass, (b) rice field Y1, (c) rice field Y2, (d) peach grove and (e) olives grove, and (f) sensible heat flux estimates over the nectarine grove vs the reference for all the data.

5. Summary and Concluding Remarks

A SR analysis based on small eddies has been proposed that allows estimating the friction velocity from the temperature trace and the mean wind speed. On this basis, the equation to estimate the surface heat flux offers advantages with respect to formulation based on MOST and earlier SR analysis. The SR method is exempt of calibration, and the zero-plane displacement is the only canopy parameter required as input. In particular, for estimating the friction velocity during near-neutral conditions, the zero-plane displacement is not required as an input when the reference height is located in the inertial sublayer or at the canopy top. The results obtained show that, in practice, its estimation can be also omitted for unstable cases because no iteration was required (i.e., the stability parameter is not involved). It is concluded that the SR analysis based on the smallest eddies is exempt of calibration, at most the canopy parameter involved is the zero-plane displacement and that it may be considered as an alternative to the EC method for applied research, such as model calibration and estimation of water requirements in agriculture, and to fill gaps in EC series.

Appendix A: Shape Parameter α-Based Formulation to Estimate the Friction Velocity, the Roughness Sublayer Depth for the Transfer of Momentum and Heat and the Turbulent Prandtl Number in the Roughness Sublayer

Some crucial equations for estimating the friction velocity required support by data. Therefore, it is worth advancing that some results shown in section 4.2 were used here and the assumptions made for estimating the friction velocity were the following.

A multitude of small whirling parcels of air, or small eddies (in the following termed fluid elements), are generated within the canopy when a macroparcel of air following a coherent motion is swept into the canopy. By continuity, when the macroparcel of air ejects into the atmospheric surface layer, most fluid elements remain attached and, therefore, a collection of fluid elements broadly spread into the surface sublayer (Zhu et al., 2007). The temperature of the air sampled at high frequency at a given measurement height (i.e., inside and above the canopy) show small fluctuations (signatures of the fluids elements) embedded in large ramp-like events (signatures of coherent structures), and it will be assumed that the actual probability distribution function for the time duration of the small fluctuations follows equation (1). Equation (1) is skewed toward the smaller exposures and the flow becomes more turbulent for higher skewness (Seo & Lee, 1988). For a given mean exposure, the smaller the shape parameter α the more skewed is equation (1). On the basis that temperature ramp periods of coherent structures and the mean shear are related (Chen et al., 1997b; Paw U et al., 1992) and that α is an eddy spectrum coefficient, it is proposed that the shape parameter α (determined from air temperature traces) and the square root of the Reynolds stress over the mean wind velocity are inversely proportional, regardless of the measurement height above the ground.

A1. The Friction Velocity in the Inertial Sublayer

A relationship between the friction velocity (u_*) and α near-neutral conditions is proposed as

$$u_{*n} = \frac{\mu\, u}{\alpha}, \tag{A1}$$

where n denotes neutral case and μ is a coefficient to be determined. Setting μ to 0.4, friction velocity estimates obtained in near neutral conditions from equation (A1) were close to the values measured using the EC method (Table 2), which suggests that μ is close to the Von Kármán constant (k). Thus, combining equation (A1) and the wind log-law $\left(\text{i.e.,}\frac{du}{dz} = \frac{u_*}{kz}\right)$ the shape parameter α can be expressed as; $\alpha = \ln\left(\frac{Z-d}{z_{0m}}\right)$, where Z is the reference height above the ground, d is the zero-plane displacement, and z_{0m} is the roughness length for momentum. On the other hand, combining equation (A1), the wind log-law and the wind power law $\left(\text{i.e.,}\frac{du}{u} = p\frac{dZ}{Z}\right)$, the parameter p can be estimated measuring the temperature of the air at high frequency, $p = \frac{1}{\alpha}$. However, instead of setting $\mu = k$, it is proposed to parameterize the coefficient μ as, $\mu = \frac{k}{\mathrm{Pr}_n}$ where Pr_n denotes the turbulent Prandtl number (Pr) for near-neutral conditions, which in the inertial sublayer is close to one (Leclerc & Foken, 2014). The turbulent Prandtl number, defined as the ratio between the eddy diffusivity for momentum and heat, has been included because the shape parameter α is determined from temperature traces. Accordingly, on the basis of MOST, the following general expression is proposed to estimate the friction velocity in the inertial sublayer

$$u_* = \frac{k\, u}{\alpha\, \mathrm{Pr}_n}\, \phi^{-1}_{m\left(\frac{(Z-d)}{L}\right)}, \tag{A2}$$

where $Pr_n = 1$ and L is the Obukhov length and $\phi_{m\,(\varsigma)} = \begin{cases} (1-16\varsigma)^{-1/4} & \text{for } \varsigma \leq 0 \\ (1+5\,\varsigma) & \text{for } \varsigma \geq 0 \end{cases}$ (Dyer, 1974) is the stability function for transfer of momentum valid in the inertial sublayer.

A2. The Friction Velocity Determined in the Roughness Sublayer

In the roughness sublayer a crucial length scale (the shear scale, L_s) is (Raupach et al., 1996)

$$L_s = \frac{u_{z=h_c}}{\mathrm{d}u/\mathrm{d}z}, \tag{A3}$$

where h_c is the canopy height. Therefore, a generalized expression for the friction velocity is

$$u_* = \frac{k\,u}{\alpha\,\mathrm{Pr}_n}\varphi^{-1}_{m\left(\frac{(Z-d)}{L},\ \frac{(Z-d)}{L_s}\right)}\ , \tag{A4}$$

where $\varphi_{m\left(\frac{(Z-d)}{L},\ \frac{(Z-d)}{L_s}\right)}$ is a stability function for the transfer of momentum. Traditionally, the analytical form for $\varphi_{m\left(\frac{(Z-d)}{L},\ \frac{(Z-d)}{L_s}\right)}$ has been expressed as (Cellier & Brunet, 1992)

$$\varphi_{m\left(\frac{(Z-d)}{L},\ \frac{(Z-d)}{L_s}\right)} = \phi^*_{m\left(\frac{Z-d}{L_s}\right)}\phi_{m\left(\frac{Z-d}{L}\right)}, \tag{A5}$$

where $\phi^{*-1}_{m\left(\frac{Z-d}{L_s}\right)}$ is the enhancement for momentum required to adapt MOST formulation in the roughness sublayer. The Obukhov length is involved in equation (A5), and therefore, the surface heat flux must be estimated which implies that the stability function for heat transfer $\varphi_{h\left(\frac{(Z-d)}{L},\ \frac{(Z-d)}{L_s}\right)}$ is involved. The latter can be written as

$$\varphi_{h\left(\frac{(Z-d)}{L},\ \frac{(Z-d)}{L_s}\right)} = \phi^*_{h\left(\frac{Z-d}{L_s}\right)}\phi_{h\left(\frac{Z-d}{L}\right)}, \tag{A6}$$

where $\phi_{h\ \left(\frac{(Z-d)}{L}\right)}$ is the stability function valid in the inertial sub-layer $\phi_{h\ (\varsigma)} = \begin{cases} \phi^2_{m\ (\varsigma)} & for\ \varsigma \leq 0 \\ \phi_{m\ (\varsigma)} & for\ \varsigma \geq 0 \end{cases}$ (Dyer, 1974) and $\phi^*_{h\ (\varsigma)}$ is the enhancement required to adapt $\phi_{h\ (\varsigma)}$in the roughness sublayer.

For the neutral case, $\varphi_{m\left(\frac{(Z-d)}{L},\ \frac{(Z-d)}{L_s}\right)} = \phi^*_{m\left(\frac{Z-d}{L_s}\right)}$, $\varphi_{h\left(\frac{(Z-d)}{L},\ \frac{(Z-d)}{L_s}\right)} = \phi^*_{h\left(\frac{Z-d}{L_s}\right)}$; and Pr_n can be expressed as $\mathrm{Pr}_n = \frac{\phi^{*-1}_m}{\phi^{*-1}_h}$. Thus, equation (A4) can be rewritten as

$$u_* = \frac{k\,u}{\alpha}\phi^{*-1}_{h\left(\frac{Z-d}{L_s}\right)}\phi^{-1}_{m\left(\frac{Z-d}{L}\right)}\ , \tag{A7}$$

which is valid for $h_c \leq Z \leq Z^*_m$ where h_c is the canopy height and Z^*_m is the roughness sublayer depth for momentum. The following formulation is adopted to estimate $\phi^*_{h\left(\frac{Z-d}{L_s}\right)}$ (Cellier & Brunet, 1992; Mölder et al., 1999)

$$\phi^*_h = \begin{cases} \left(\dfrac{Z-d}{Z^*_h-d}\right) for\ Z < Z^*_h \\ 1 \qquad\qquad for\ Z \geq Z^*_h \end{cases}, \tag{A8}$$

where Z^*_h is the roughness sublayer depth for heat transfer.

A3. Estimation of the Roughness Sublayer Depth for Momentum and Heat Transfer

Equations (A3)–(A8) allows expressing the shear-scale L_s as

$$\frac{1}{L_s} = \left.\frac{\mathrm{d}(\ln\alpha)}{\mathrm{d}z}\right|_{z=h_c} + \left.\frac{1}{\phi^*_h}\frac{d\phi^*_h}{dz}\right|_{z=h_c} + \left.\frac{1}{\phi_m}\frac{d\phi_m}{dz}\right|_{z=h_c} \tag{A9}$$

Inside the canopy, from about the zero-plane displacement up to the canopy top both the horizontal mean wind speed normalized by u_{h_c} and the Reynolds stress $(-\overline{u'w'})$ normalized by u^2_* show an exponential decay versus Z/h_c (Kaimal & Finnigan, 1994; Leclerc & Foken, 2014). Therefore, by assuming that u^2 is proportional to $\left(-\overline{u'w'}\right)\alpha^2$, $\left(\frac{u}{u_{h_c}}\right)^2$ would be related with $\frac{-\overline{u'w'}}{u^2_*}\left(\frac{u_*}{u_{h_c}}\alpha\right)^2$, which suggest that the shape parameter α profile also follows an exponential decay versus Z/h_c. The α profile in a tree orchard (Figure 6) shows that α decays

versus Z/h_c in the crown. It allows proposing that the natural log of α decays rather linear versus Z/h_c with a slope, $\left.\frac{\mathrm{d}(\ln\alpha)}{dz}\right|_{z=h_c}$, that may be estimated as $\frac{\ln(\alpha_{z=h_c})-\ln(\alpha_{z=d})}{(h_c-d)}$ because below the zero-plane displacement the α profile appears unpredictable (Figure 6).

A4. Estimating $\ln(\alpha_{z=h_c})$ and $\ln(\alpha_{z=d})$ Near-Neutral Conditions

Within the roughness sublayer (above the canopy), the shape parameter α determined near-neutral conditions was around 3.25 (Figures 7). Thus, taking an intermediate value for $\alpha_{z=h_c}$ close to 3.25, a representative value for $\ln(\alpha_{z=h_c})$ near-neutral conditions of about 1.15 may be expected. It is of interest to note that for an α value of about 3.25 at the canopy top suggests that the expected value for $\frac{u_*}{u_{h_c}}\alpha$ is close to one (Graefe, 2004) and, therefore, that $\left(\frac{u}{u_{h_c}}\right)^2$ is close to $\frac{-\overline{u'w'}}{u_*^2}\left(\frac{u_*}{u_{h_c}}\alpha\right)^2$.

Inside the canopy, a rough estimation of $\ln(\alpha_{z=d})$ near-neutral conditions can be obtained by assuming that $\left(\frac{u}{u_{h_c}}\right)^2$ is close to $\frac{-\overline{u'w'}}{u_*^2}\left(\frac{u_*}{u_{h_c}}\alpha\right)^2$, as follows. For contrasting canopies, at $Z/h_c = 0.7$ (i.e., at a height close to the zero-plane displacement) it was found that on average both $\frac{u}{u_{h_c}}$ and $\frac{-\overline{u'w'}}{u_*^2}$ were about 0.5 (Florens et al., 2013; Kaimal & Finnigan, 1994). Consequently, because an intermediate value for $\frac{u_*}{u_{h_c}}$ is about one third (Graefe, 2004), the relationship $\left(\frac{u}{u_{h_c}}\right)^2 \approx \frac{-\overline{u'w'}}{u_*^2}\left(\frac{u_*}{u_{h_c}}\alpha\right)^2$ suggests that a representative value for $\ln(\alpha_{z=d})$ is about 0.75.

In equation (A9), by virtue of equation (A2) the term $\left.\frac{1}{\phi_m}\frac{d\phi_m}{dz}\right|_{z=h_c}$ can be expressed as $\left.\frac{1}{\phi_m}\frac{d\phi_m}{dz}\right|_{z=h_c}$ $= \begin{cases} \frac{-\varsigma_{h_c}}{4\left(1-16\varsigma_{h_c}\right)(h_c-d)} & \text{for } \varsigma_h \le 0 \\ \frac{5\varsigma_{h_c}}{\left(1+\varsigma_{h_c}\right)(h_c-d)} & \text{for } \varsigma_h \ge 0 \end{cases}$ where $\varsigma_{h_c} = \frac{(h_c-d)}{L}$ and by virtue of equation (A8) the term $\left.\frac{1}{\phi_h^*}\frac{d\phi_h^*}{dz}\right|_{z=h_c}$ is $\frac{1}{(h_c-d)}$. Thus, near-neutral conditions $\left.\frac{\mathrm{d}(\ln\alpha)}{\mathrm{dz}}\right|_{z=h_c} + \left.\frac{1}{\phi_h^*}\frac{\mathrm{d}\phi_h^*}{\mathrm{dz}}\right|_{z=h_c} + \frac{1}{\phi_m}\left.\frac{\mathrm{d}\phi_m}{\mathrm{dz}}\right|_{z=h_c}$ in Equation (A9) roughly approaches $\frac{1}{L_s}$ to, $\frac{1}{L_s} = \frac{\ln(\alpha_{Z=h_c})}{(h_c-d)}$. For field applications (i.e, for convenience), by assuming that the shape parameter α remains fairly constant in the roughness sublayer, it is proposed to estimate the shear-scale L_s regardless of the stability case as

$$L_s = \frac{(h_c-d)}{\ln(\alpha_Z)}. \tag{A10}$$

Noteworthy that equation (A10) proposes that the shear scale can be estimated without taking measurements of the wind speed or characteristic canopy parameters such as the leaf area index and dimensions related with the architecture of the canopy (Graefe, 2004).

The roughness sublayer depth (above the zero-plane displacement) for momentum and heat (Z_h^*) can be estimated, respectively, as (Leclerc & Foken, 2014; Mölder et al., 1999; Raupach et al., 1996)

$$\left(Z_m^*-d\right) = (h_c-d) + 2L_s \text{ and } \left(Z_h^*-d\right) = (h_c-d) + 3L_s \tag{A11}$$

that using equation (A10) allows rewriting equation (A11) as

$$Z_m^*-d = (h_c-d)\left[\frac{2+\ln(\alpha_Z)}{\ln(\alpha_Z)}\right] \text{ and } Z_h^*-d = (h_c-d)\left[\frac{3+\ln(\alpha_Z)}{\ln(\alpha_Z)}\right], \tag{A12}$$

which can be combined with equation (A8) to express to rewrite ϕ_h^* as

$$\phi_h^* = \frac{(Z-d)}{(h-d)}\left[\frac{\ln(\alpha_Z)}{3+\ln(\alpha_Z)}\right]. \tag{A13}$$

Though indirectly, equation (A12) supports the assumption made in equation (A10) (i.e., α remains fairly constant versus height near-neutral conditions in the roughness sublayer) as follows. Taking the intermediate α value, $\alpha = 3.25$, as input in equation (A12) to estimate the top of the roughness sublayers for momentum and heat transfer, the ratios obtained for $\frac{Z_m^*}{h_c}$ and $\frac{Z_h^*}{h_c}$ using $d = 2/3h_c$ are $\frac{Z_m^*}{h_c} = 1.60$ and $\frac{Z_h^*}{h_c} = 1.85$, respectively. For momentum, the ratio obtained was similar to that used by Rannik et al. (2003), $\frac{Z_m^*}{h_c} = 1.66$, and to an expected ratio determined by Florens et al. (2013), $\frac{Z_m^*}{h_c} = 1.5$. Though the ratios obtained either for momentum and heat underestimated the values reported in different experiments (Graefe, 2004) or the traditional ratio $\frac{Z_m^*}{h_c} = 2$ used as a rule of thumb (Leclerc & Foken, 2014), the latter were suggested too large by Florens et al. (2013). On the other hand, parameterizing the enhancement for transfer of momentum as (Cellier & Brunet, 1992), $\phi_m^* = \begin{cases} \left(\frac{Z-d}{Z_m^*-d}\right)^{\eta} & \text{for } Z < Z_m^* \\ 1 & \text{for } Z \geq Z_m^* \end{cases}$ where $\eta = 0.61$ (Mölder et al., 1999), by virtue of equations (A12) and (A13) Pr_n expresses as

$$\mathrm{Pr}_n = \left[\frac{(z-d)}{(h_c-d)}\ln(\alpha_Z)\right]^{(1-\eta)} \frac{[2+\ln(\alpha_Z)]^{\eta}}{(3+\ln(\alpha_Z))}. \tag{A14}$$

There is a consensus that at the canopy top Pr_n is close to 0.5, which is the value predicted by equation (A14) setting $Z = h_c$, $\eta = 0.61$, and $\alpha = 3.25$. At the top of the roughness sublayer depth for the transfer of heat, $Z = Z_h^*$, the value predicted for Pr_n using $\eta = 0.61$ and $\alpha = 3.25$ is $Pr_n = 0.85$, which falls in the range of values reported (Leclerc & Foken, 2014).

Acknowledgments
The author gratefully acknowledges R. L Snyder (retired extensionist at LAWR department, UC Davis) and the late A. Martínez-Cob (1960-2014, researcher at Aula Dei, Zaragoza, Spain) who provided all the data used in this work. This work was supported under project CGL2015-65627-C3-1-R (AEI/FEDER, UE) Ministerio de Economía y Competitividad of Spain. Data sets are available at the repository of the University of Lleida, http://hdl.handle.net/10459.1/64583.

References

Arnqvist, J., & Bergström, H. (2014). Flux-profile relation with roughness sublayer correction. *Quarterly Journal of the Royal Meteorological Society*, *141*, 1191–1197.

Brent, R. P. (1973). *Algorithms for minimization without derivatives*. Englewood Cliffs, NJ: Prentice-Hall.

Brutsaert, W. (1965). A model for evaporation as a molecular diffusion process into a turbulent atmosphere. *Journal of Geophysical Research*, *70*(20), 5017–5024. https://doi.org/10.1029/JZ070i020p05017

Brutsaert, W. (1975). A theory for local evaporation (or heat transfer) from rough and smooth surfaces at ground level. *Water Resources Research*, *28*(1), 31–39. https://doi.org/10.1016/0009-2509(73)85083-3.

Brutsaert, W. (1982). Evaporation into the atmosphere. In *Environmental fluid mechanics* (p. 299). Dordrecht/Boston/London: Kluwer Academic Publishers.

Bullin, J., & Dukler, A. E. (1972). Random eddy models for surface renewal: Formulation as a stochastic process. *Chemical Engineering Science*, *27*(2), 439–442. https://doi.org/10.1016/0009-2509(72)85081-4

Castellví, F. (2004). Combining surface renewal analysis and similarity theory: A new approach for estimating sensible heat flux. *Water Resources Research*, *40*, W05201. https://doi.org/10.1029/2003WR002677

Castellví, F. (2012). Fetch requirements using surface renewal analysis for estimating scalar surface fluxes from measurements in the inertial sub-layer. *Agricultural and Forest Meteorology*, *152*, 233–239. https://doi.org/10.1016/j.agrformet.2011.10.004

Castellví, F. (2013). A method for estimating the sensible heat flux in the inertial sub-layer from high-frequency air temperature and averaged gradient measurements. *Agricultural and Forest Meteorology*, *180*, 68–75. https://doi.org/10.1016/j.agrformet.2013.05.005

Castellví, F., Consoli, S., & Papa, R. (2012). Sensible heat flux estimates using two different methods based on surface renewal analysis. A study case over an orange orchard in Sicily. *Agricultural and Forest Meteorology*, *152*, 58–64. https://doi.org/10.1016/j.agrformet.2011.09.001

Castellví, F., & Martínez-Cob, J. (2005). Estimating sensible heat flux using surface renewal analysis and the flux variance method: A case study over olive trees at Sastago (NE of Spain). *Water Resources Research*, *41*, W09422. https://doi.org/10.1029/2005WR004035

Castellví, F., Perez, P. J., & Ibañez, M. (2002). A method based on high frequency temperature measurements to estimate sensible heat flux avoiding the height dependence. *Water Resources Research*, *38*(6), 1084. https://doi.org/10.1029/2001WR000486

Castellví, F., & Snyder, R. L. (2009a). Combining the dissipation method and surface renewal analysis to estimate scalar fluxes from the time traces over rangeland grass near Ione (California). *Hydrological Processes*, *23*(6), 842–857. https://doi.org/10.1002/hyp.7223

Castellví, F., & Snyder, R. L. (2009b). On the performance of surface renewal analysis to estimate sensible heat flux over two growing rice fields under the influence of regional advection. *Journal of Hydrology*, *375*(3-4), 546–553. https://doi.org/10.1016/j.jhydrol.2009.07.005

Castellví, F., & Snyder, R. L. (2009c). Sensible heat flux estimates using surface renewal analysis. A study case over a peach orchard. *Agricultural and Forest Meteorology*, *149*, 1397–1402.

Castellví, F., & Snyder, R. L. (2010). A comparison between latent heat fluxes over grass using a weighing lysimeter and surface renewal analysis. *Journal of Hydrology*, *381*(3-4), 213–220. https://doi.org/10.1016/j.jhydrol.2009.11.043

Castellví, F., Snyder, R. L., & Baldocchi, D. D. (2008). Surface energy-balance closure over rangeland grass using the eddy covariance method and surface renewal analysis. *Agricultural and Forest Meteorology*, *148*(6-7), 1147–1160. https://doi.org/10.1016/j.agrformet.2008.02.012

Castellví, F., Snyder, R. L., Baldocchi, D. D., & Martınez-Cob, A. (2006). A comparison of new and existing equations for estimating sensible heat flux using surface renewal and similarity concepts. *Water Resources Research*, *42*, W08406. https://doi.org/10.1029/2005WR004642

Cellier, P., & Brunet, Y. (1992). Flux-gradient relationships above tall plant canopies. *Agricultural and Forest Meteorology*, *58*(1-2), 93–117. https://doi.org/10.1016/0168-1923(92)90113-I

Chen, W., Novak, M. D., Black, T. A., & Lee, X. (1997a). Coherent eddies and temperature structure functions for three contrasting surfaces. Part I. ramp model with finite micro-front time. *Boundary-Layer Meteorology*, *84*(1), 99–124. https://doi.org/10.1023/A:1000338817250

Chen, W., Novak, M. D., Black, T. A., & Lee, X. (1997b). Coherent eddies and temperature structure functions for three contrasting surfaces. Part II: Renewal model for sensible heat flux. *Boundary-Layer Meteorology*, *84*(1), 125–147. https://doi.org/10.1023/A:1000342918158

Danckwerts, P. (1951). Significance of liquid-film coefficients in gas absorption. *Industrial and Engineering Chemistry*, *43*(6), 1460–1467. https://doi.org/10.1021/ie50498a055

Dyer, A. J. (1974). A review of flux-profile relationships. *Boundary-Layer Meteorology*, *7*(3), 363–372. https://doi.org/10.1007/BF00240838

Florens, E., Eiff, O., & Moulin, F. (2013). Defining the roughness sublayer and its turbulence statistics. *Experiments in Fluids*, *54*(4), 1–15.

Foken, T., & Oncley, S. P. (1995). Workshop on instrumental and methodical problems of land surface flux measurements. *Bulletin of the American Meteorological Society*, *76*(7), 1191–1224. https://doi.org/10.1175/1520-0477-76.7.1191

Graefe, J. (2004). Roughness layer corrections with emphasis on SVAT model applications. *Agricultural and Forest Meteorology*, *124*(3-4), 237–251. https://doi.org/10.1016/j.agrformet.2004.01.003

Haghighi, E., & Or, D. (2013). Evaporation from porous surfaces into turbulent airflows: Coupling eddy characteristics with pore scale vapor diffusion. *Water Resources Research*, *49*, 8432–8442. https://doi.org/10.1002/2012WR013324

Harriott, P. (1962). A random eddy modification of the penetration theory. *Chemical Engineering Science*, *17*(3), 149–154. https://doi.org/10.1016/0009-2509(62)80026-8

Higbie, R. (1935). The rate of absorption of a pure gas into a still liquid during short periods of exposure. *Transactions of AIChE*, *31*, 365–388.

Jackson, P. S. (1981). On the displacement height in the logarithmic velocity profile. *Journal of Fluid Mechanics*, *111*(1), 15–25. https://doi.org/10.1017/S0022112081002279

Kaimal, J. C., & Finnigan, J. J. (1994). *Atmospheric boundary layer flows: Their structure and measurement* (289 pp.). New York: Oxford University Press.

Katul, G. G., Hsieh, C.-I., Oren, R., Ellsworth, D., & Philips, N. (1996). Latent and sensible heat flux predictions from a uniform pine forest using surface renewal and flux variance methods. *Boundary-Layer Meteorology*, *80*(3), 249–282. https://doi.org/10.1007/BF00119545

Katul, G. G., & Liu, H. (2017). A Kolmogorov-Brutsaert structure function model for evaporation into a turbulent atmosphere. *Water Resources Research*, *53*, 3635–3644. https://doi.org/10.1002/2016WR020006

Leclerc, M. Y., & Foken, T. (2014). *Footprints in micrometeorology and ecology*. Berlin, Heidelberg: Springer-Verlag. https://doi.org/10.1007/978-3-642-54545-0_2

Mauder, M., & Foken, T. (2004). Documentation and instruction manual of the eddy covariance software package TK2. Universität Bayreuth, Abt. Mikrometeorologie, Arbeitsergebnisse, *26* (44 pp.), (Print: ISSN 1614–8916; Internet: ISSN 1614–8926).

Mauder, M., Oncley, S. P., Vogt, R., Weidinger, T., Ribeiro, L., Bernhofer, C., Foken, T., et al. (2007). The energy balance experiment EBEX-2000. Part II: Intercomparison of eddy-covariance sensors and post-field data processing methods. *Boundary-Layer Meteorology*, *123*(1), 29–54. https://doi.org/10.1007/s10546-006-9139-4

Meek, R. L., & Baer, A. L. (1970). The periodic viscous sublayer in turbulent flow. *AICHE Journal*, *16*(5), 841–848. https://doi.org/10.1002/aic.690160525

Mölder, M., Grelle, A., Lindroth, A., & Halldin, S. (1999). Flux profile relationships over a boreal forest roughness sublayer corrections. *Agricultural and Forest Meteorology*, *98*(99), 645–658.

Nash, J. C. (1990). *Compact numerical methods for computers: Linear algebra and function minimization* (2nd ed.). New York: Adam Hilger Bristol (ENG).

Paw U, K. T., Baldocchi, D. D., Meyers, T. P., & Wilson, K. B. (2000). Correction of eddy-covariance measurements incorporating both advective effects and density fluxes. *Boundary-Layer Meteorology*, *97*(3), 487–511. https://doi.org/10.1023/A:1002786702909

Paw U, K. T., Brunet, Y., Collineau, S., Shaw, R. H., Maitani, T., Qui, J., & Hipps, L. (1992). On coherent structures in turbulence above and within agricultural plant canopies. *Agricultural and Forest Meteorology*, *61*, 55–68. https://doi.org/10.1016/0168-1923(92)90025-Y

Paw U, K. T., Qiu, J., Su, H.-B., Watanabe, T., & Brunet, Y. (1995). Surface renewal analysis: A new method to obtain scalar fluxes without velocity data. *Agricultural and Forest Meteorology*, *74*, 119–137.

Qiu, J., Paw U, K. T., & Shaw, R. H. (1995). Pseudo-Wavelet analysis of turbulence patterns in three vegetations layers. *Boundary-Layer Meteorology*, *72*, 177–204.

Rannik, Ü., Markkanen, T., Raittila, T., Hari, P., & Vesala, T. (2003). Turbulence statistics inside and above forest: Influence on footprint prediction. *Boundary-Layer Meteorology*, *109*, 163–189. https://doi.org/10.1023/A:1025404923169

Raupach, M. R. (1994). Simplified expressions for vegetation roughness length and zero-plane displacement as functions of canopy height and area index. *Boundary-Layer Meteorology*, *71*(1–2), 211–216. https://doi.org/10.1007/BF00709229

Raupach, M. R., Finnigan, J. J., & Brunet, Y. (1996). Coherent eddies in vegetation canopies: The mixing-layer analogy. *Boundary-Layer Meteorology*, *78*(3-4), 351–382. https://doi.org/10.1007/BF00120941

Seo, Y. G., & Lee, W. K. (1988). Single-eddy model for random surface renewal. *Chemical Engineering Science*, *43*(6), 1395–1402. https://doi.org/10.1016/0009-2509(88) 85112-1

Shapland, T. M., McElrone, A. J., Snyder, R. L., & Paw U, K. T. (2012a). Structure function analysis of two-scale scalar ramps. Part I: Theory and modelling. *Boundary-Layer Meteorology*, *145*(1), 5–25. https://doi.org/10.1007/s10546-012-9742-5

Shapland, T. M., McElrone, A. J., Snyder, R. L., & Paw U, K. T. (2012b). Structure function analysis of two-scale scalar ramps. Part II: Ramp characteristics and surface renewal flux estimation. *Boundary-Layer Meteorology*, *145*(1), 27–44. https://doi.org/10.1007/s10546-012-9740-7

Snyder, R. L., Spano, D., & Paw U, K. T. (1996). Surface renewal analysis for sensible and latent heat flux density. *Boundary-Layer Meteorology*, *77*(3-4), 249–266. https://doi.org/10.1007/BF00123527

Suvočarev, K., Shapland, T. M., Snyder, R. L., & Martínez-Cob, A. (2014). Surface renewal performance to independently estimate sensible and latent heat fluxes in heterogeneous crop surfaces. *Journal of Hydrology*, *509*, 83–93. https://doi.org/10.1016/j.jhydrol.2013.11.025

Van Atta, C. W. (1977). Effect of coherent structures on structure functions of temperature in the atmospheric boundary layer. *Archives of Mechanics*, *29*, 161–171.

Zhu, W., Van Hout, R., & Katz, J. (2007). On the flow structure and turbulence during sweep and ejection events in a wind-tunnel model canopy. *Boundary-Layer Meteorology*, *124*(2), 205–233. https://doi.org/10.1007/s10546-007-9174-9